Journal of *Marine Science and Engineering*

MDPI

Article

Trawling-Induced Sedimentary Dynamics in Submarine Canyons of the Gulf of Palermo (SW Mediterranean Sea)

Marta Arjona-Camas [1,2,*], Claudio Lo Iacono [1], Pere Puig [1], Tommaso Russo [3] and Albert Palanques [1]

[1] Institute of Marine Sciences (CSIC), Passeig Marítim de la Barceloneta, 37-49, 08003 Barcelona, Spain; loiacono@icm.csic.es (C.L.I.); ppuig@icm.csic.es (P.P.); albertp@icm.csic.es (A.P.)
[2] Departament de Dinàmica de la Terra i de l'Oceà, Facultat de Ciències de la Terra, Universitat de Barcelona, c/Martí i Franquès s/n, 08028 Barcelona, Spain
[3] Laboratory of Experimental Ecology and Aquaculture, Department of Biology, University of Rome Tor Vergata, Via Cracova 1, 00133 Rome, Italy; tommaso.russo@uniroma2.it
* Correspondence: marjona@ub.edu

Abstract: Bottom trawling in submarine canyons can affect their sedimentary dynamics, but studies addressing this topic are still scarce. In the Gulf of Palermo (NW Sicily, SW Mediterranean Sea), bottom trawling occurs on the continental slope, but principally concentrates within Oreto Canyon. Hydrographic profiles and time series data of temperature, turbidity, and currents obtained by a CTD probe and by moored instruments, respectively, revealed increased turbidity values and the presence of bottom and intermediate nepheloid layers coinciding with periods of bottom trawling activity. The delay between the onset of trawling activities along the Oreto canyon axis and the increase in water turbidity at the mooring location indicate that trawling resuspended particles are progressively advected down-canyon by hydrodynamic processes. Topographic waves and near-inertial currents seem to contribute to the sediment transport of resuspended particles as bottom and intermediate nepheloid layers. Results presented in this paper highlight the complex relationship between hydrodynamic processes and sediment resuspension by trawling in submarine canyons.

Keywords: submarine canyons; bottom trawling; turbidity; nepheloid layers; hydrodynamics; Mediterranean Sea

Citation: Arjona-Camas, M.; Lo Iacono, C.; Puig, P.; Russo, T.; Palanques, A. Trawling-Induced Sedimentary Dynamics in Submarine Canyons of the Gulf of Palermo (SW Mediterranean Sea). *J. Mar. Sci. Eng.* **2024**, *12*, 1050. https://doi.org/10.3390/jmse12071050

Academic Editor: Dimitris Sakellariou

Received: 9 May 2024
Revised: 14 June 2024
Accepted: 20 June 2024
Published: 22 June 2024

1. Introduction

Submarine canyons are morphological features that incise the continental margins worldwide [1]. They are important pathways for the transfer of water, sediments, and pollutants between coastal areas and deep-sea environments, particularly during high-energy natural events such as slope failures, river floods, wave-storms, and cascading of dense shelf waters [2–6]. The morphology of submarine canyons gives rise to complex physical and oceanographic conditions that locally increase biological productivity and diversity [7,8]. Combined with the enhanced particulate matter fluxes that occur in their interior, canyons also serve as spawning areas for many pelagic and benthic species of commercial interest [9,10]. In consequence, submarine canyon environments are increasingly targeted by commercial fishing vessels, including bottom trawlers [11].

There is now evidence that sedimentary transport dynamics in the marine environment can be altered by bottom trawling activities, since the contact of the net and the heavy trawl doors with the seafloor can resuspend large volumes of sediment [12–17]. Several studies have shown that when this type of fishery occurs in areas within and around submarine canyons, sediment resuspended by bottom trawl gears can be transferred towards deeper canyon areas as diluted sediment gravity flows [13,18–20], or as enhanced near-bottom nepheloid layers (BNLs) that can evolve into intermediate nepheloid layers (INLs) detached at different water levels [13,21–24]. In consequence, the alterations of the

sedimentary dynamics by bottom trawling activities can generate anthropogenic sedimentary depocenters along submarine canyon axes, which have been mostly documented in the NW Mediterranean Sea [25–29].

The Gulf of Palermo, NW Sicily (SW Mediterranean Sea), is incised by many submarine canyons [30,31], and in this margin, bottom trawling activities occur on the outer shelf and upper slope areas surrounding the head of submarine canyons, but it mainly concentrates along the axis of the Oreto Canyon (Figure 1) [32]. In this area, it has been recently demonstrated that this anthropogenic activity has also increased sedimentation rates by some orders of magnitude inside various submarine canyon axes (i.e., Oreto, Arenella, and Eleuterio Canyons), modifying their natural sedimentary regimes [32,33]. Other than that, there are only a few studies regarding the modern sedimentary dynamics in this margin, but they are scarce and limited to the continental shelf [34,35]. Hence, the main goal of this work is to assess the contemporary sediment transport mechanisms along the Oreto Canyon and investigate how bottom trawling activities can alter the water turbidity and sediment transport dynamics within it. This has been accomplished by analyzing time series of turbidity, temperature, and currents from moored instruments deployed in the deeper sector of the Oreto Canyon, in combination with data from hydrographic transects conducted over the study area. Vessel Monitoring System (VMS) data have also been used in order to map the fishing effort of the study area and assess the tracks of bottom trawling vessels in the Gulf of Palermo at the time of the instrumented mooring deployment.

2. Materials and Methods

2.1. Study Area

2.1.1. Geological Setting

The Gulf of Palermo is located in the northwestern sector of the Sicilian continental margin and is enclosed by Cape Gallo to the northwest and Cape Zafferano to the southeast (Figure 1). Two rivers, the Oreto and the Eleuterio, cross the Palermo coastal plain and flow into the gulf, with an average discharge of 0.25 $m^3 \cdot s^{-1}$ that can reach maximum values of 5.3 $m^3 \cdot s^{-1}$ and 26.3 $m^3 \cdot s^{-1}$ during storm events, respectively [36].

The continental shelf of this gulf occupies a total area of 250 km^2 and is 8 km wide on average, narrowing to 2.5 km in its westernmost sector [30]. Sediment grain size is coarser towards the northwest of the continental shelf and at the river mouths discharging into the gulf, mainly consisting of sand. The sediment grain size distribution shows a general fining trend towards the southeast, following the general path of the current [37]. The continental shelf edge is located at a depth of 115–125 m and is intended by the head of five sinuous to linear submarine canyons (Mondello, Addaura, Arenella, Oreto, and Eleuterio Canyons), with slope gradients ranging from 6 to 13°, which extend downslope until reaching maximum depths of 1500 m at the Palermo basin plain [30] (Figure 1).

The most extensive submarine canyons in the Gulf of Palermo are the Oreto and Eleuterio Canyons, which incise the central and eastern sectors of this gulf (Figure 1). The Oreto Canyon presents a sinuous path that incises the shelf edge at a depth of 120 m, and its development has been related to sediment inputs from the Oreto River during the Late Quaternary Sea level low-stand stages [30]. This canyon presents a V-shaped thalweg and widens to a maximum of 270 m downslope from a 750 m deep structural topographic obstacle [30]. Analyses of sediment cores collected in the Oreto canyon axis reveal a composition of mostly silt (~51%) and clay (~47%), and low amounts of sand (2%) [32]. The head of the Eleuterio Canyon develops very close to the headland in front of Cape Zafferano (Figure 1), and probably captures most of the eastward longshore currents of the gulf, steered by the narrowing of the continental shelf and by the actual geometry of the coast [30,31]. The Mondello, Addaura, and Arenella submarine canyons are located at the western sector of the gulf and incise a narrower continental shelf (Figure 1). In contrast to the Oreto and Eleuterio Canyons, these canyons are steeper (slope gradients up to 13°) and shorter, and their evolution has been related to slope mass failures retrograding from the deeper slope domains towards shallower depths [30].

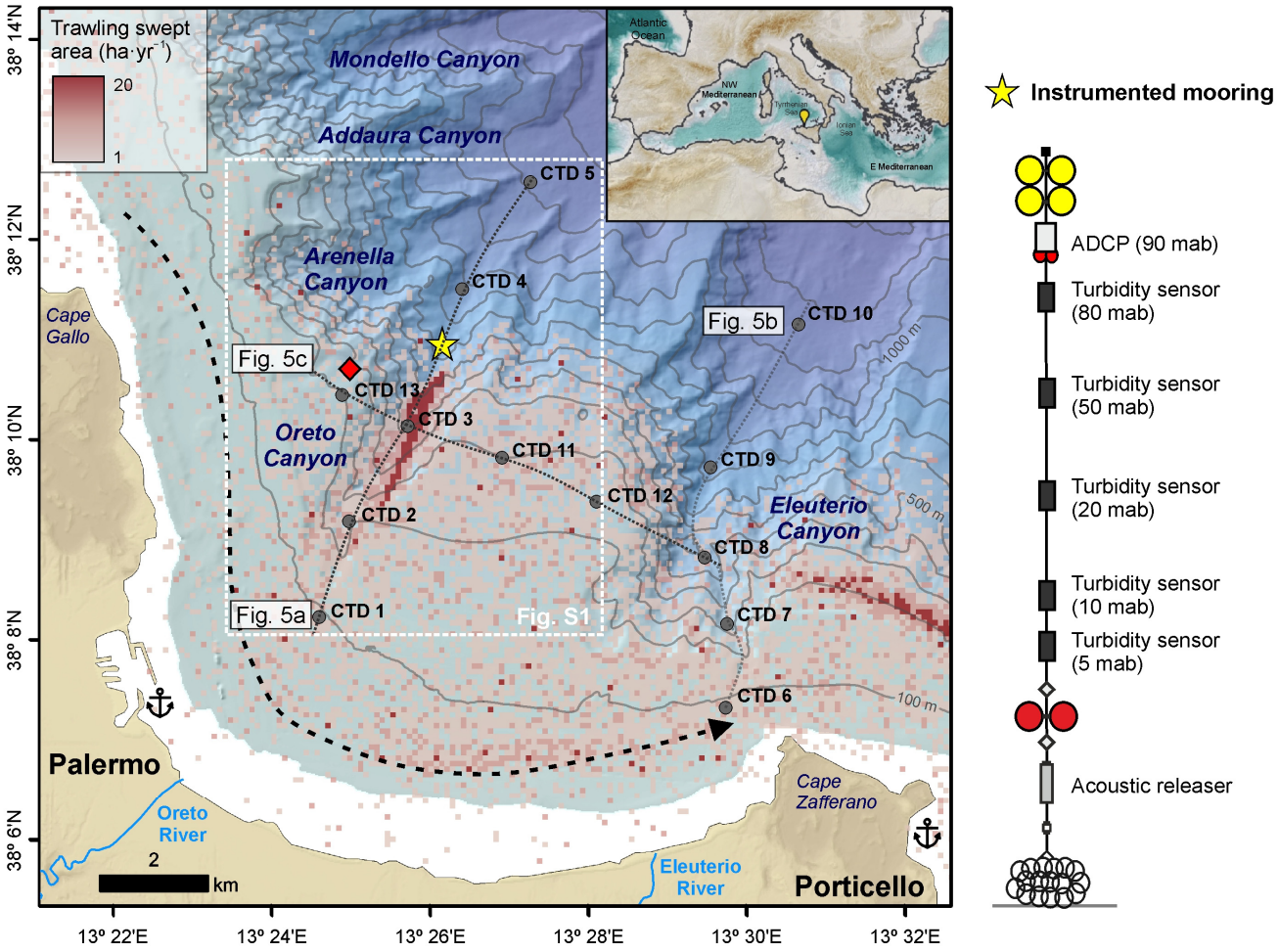

Figure 1. Bathymetric map of the Gulf of Palermo, showing the location of the main submarine canyons incising the margin (Mondello, Addaura, Arenella, Oreto, and Eleuterio), as well as the instrumented mooring line (yellow star) and the CTD stations sampled (grey dots). The red diamond shows the location of the Med-WAV model's grid point, from which wave conditions have been retrieved. The overlying density raster represents the mean annual trawling intensity as swept area per year (ha·yr^{-1}) obtained from Vessel Monitoring System (VMS) data between 2008 and 2016. The location of the main harbors (Palermo and Porticello) and the most important rivers discharging into the Gulf of Palermo are also given. The black dashed line shows the direction of the regional current over the study area, which flows along the continental margin. Bathymetric contour lines are displayed every 100 m. The bathymetric data used in this paper were acquired during the course of three oceanographic cruises in 2001, 2004 (CARG cruises), and 2009 (MaGIC cruise) (www.isprambiente.it (accessed on 1 May 2023); [38]. Also, the scheme of the instrumented mooring line deployed in the axis of the Oreto Canyon at 750 m depth is shown. The mooring includes a downward-looking 300 kHz Acoustic Doppler Current Profiler (ADCP) and a string of turbidimeters. The position of the instruments along the line, expressed in meters above the bottom (mab), is illustrative of the general mooring design, as they are not scaled.

2.1.2. Oceanographic Setting

The Gulf of Palermo is characterized by strong seasonal variations of oceanographic processes [39]. The area is dominated by an eastward flowing geostrophic thermohaline circulation, mainly involving three water masses: the Modified Atlantic Water (MAW), the Levantine Intermediate Water (LIW), and the Tyrrhenian Deep Water (TDW) [40,41].

The MAW is usually found in this margin between the surface and approximately 200 m water depth (core depth 0–100 m), and it originates from the surface inflow of

the Atlantic Water into the Mediterranean Sea through the Strait of Gibraltar [42]. Its hydrographic properties undergo chemical and physical modifications, as well as mixing processes, by evaporation and by the entrainment of Mediterranean water during its path along the North African coastline [40,42]. This water mass normally presents salinities lower than 38.0 and temperatures between 14 and 15 °C, although these properties can vary along its cyclonic flow along the Mediterranean Sea [42]. Directly beneath, the LIW is approximately found between 200 and 700 m water depth (core depth 300–500 m). It is formed during winter periods in the Eastern Mediterranean basin due to meteorological factors, when dry, cold, and strong winds enhance mixing and evaporation, leading to vertical convection processes [43]. The LIW circulates westwards through both eastern and western Mediterranean basins, contributing predominantly to the outflow from the Gibraltar Strait to the Atlantic Ocean [44]. Its salinities can reach up to 38.8 with maximum temperatures of 15.5 °C [45]. Both surface and intermediate water masses in the Tyrrhenian Sea basically follow a cyclonic circulation pattern along the Sicilian and Italian shelves [46], although small but quasi-permanent gyres are also present [47,48]. In its deeper part, the water column is occupied by the Tyrrhenian Deep Water (TDW), which is defined to be a mixing product of the Western Mediterranean Deep Water (WMDW) from the Sicily Channel and the LIW above it [49] flowing out from the Sardinia Channel [50]. However, the processes responsible for the formation of this TDW and the actual water masses involved are still the subject of debate [46,51,52].

Oceanographically, this region is affected by sporadic winter storms from the NW, NE, and E, as well as by a seasonal wind-driven coastal current, described as the Tyrrhenian Sicilian Current (TSC) [53]. This current flows eastward, with maximum velocities of 0.9 knots [54].

2.1.3. Bottom Trawling Grounds

The Gulf of Palermo has held bottom trawling grounds for local trawlers for more than 50 years. Bottom trawlers in this gulf operate using "otter trawl" gear, which consists of dragging a wide net over the stern that is kept open horizontally and in contact with the seafloor by two otter boards [13].

During the 1950s, engine-propelled trawl vessels began to fish in this gulf, although it was not until the 1960s and 1970s when the size of the fishing fleets, mainly from Porticello and Palermo harbors, rapidly increased. However, they did not exceed 200 horsepower (HP) average engine power and mainly operated in shelf waters [32]. The industrialization of bottom trawling fleets occurred in the late 1980s and allowed them to exploit deeper fishing grounds using more powerful engines (500–2000 HP). Bottom trawling became more concentrated on the outer shelf and upper slope sectors of the gulf, and on the Oreto Canyon axis [32]. Concurrent with the expansion of fishing fleets to deeper fishing grounds in the late 1980s, natural sedimentation rates within submarine canyon axes increased by one order of magnitude [32,33]. Nowadays, trawling grounds in the Gulf of Palermo mainly concentrate on the outer shelf and upper slope sectors between Oreto and Eleuterio submarine canyons (Figure 1). The available fishing data on the region indicate that trawl hauls at the continental margin are conducted between ~50 and ~700 m depth, following the bathymetric contours. However, the highest trawling effort is concentrated along the axis of the Oreto Canyon, where trawlers perform hauls between ~200 and 700 m depth (Figure 1). In contrast, the axes of other submarine canyons incising the margin remain untrawled (Figure 1).

2.2. Sampling

In the framework of the Eurofleets-2 ISLAND (Exploring SiciLian CAnyoN Dynamics) cruise onboard the R/V *Ángeles Alvariño*, an instrumented mooring line was deployed in the axis of the Oreto Canyon at 750 m depth (latitude: 38°10.98′ N; longitude: 013°26.03′ E) on 8 August 2016 (Figures1 and S1). The mooring line was equipped with a string of 5 turbidimeters (AQUA logger 210TY, AQUATEC, Basingstoke, UK) at 5, 10, 20, 50, and

80 m above the bottom (mab), programmed to measure turbidity, expressed in Formazin Turbidity Units (FTU), at 2 min sampling intervals. The loggers were set to operate in auto-gain mode, meaning that they go over different gains at the time of measuring and automatically select a suitable range that does not saturate the signal. The mooring line was also equipped with a downward-looking 300 kHz Acoustic Doppler Current Profiler (ADCP) (Teledyne RDI, Poway, CA, USA) placed at 90 mab, above the turbidimeters, which was configured with vertically stacked cells of 2 m thickness and a sampling interval of 5 min (see mooring schematics in Figure 1). The mooring line was retrieved on 13 January 2017, using a sailboat, and the instruments collected data for five months.

During the ISLAND cruise, three ship-based hydrographic transects were also conducted in the study area. The hydrographic data were collected using a SeaBird 9 CTD probe coupled with a SeaPoint turbidity sensor (Sea-Bird Scientific, Bellevue, WA, USA). The first transect, conducted on 15 August 2016, consisted of 5 vertical CTD stations along the axis of the trawled Oreto Canyon. The second transect was conducted on 16 August and consisted of 5 vertical CTD stations along the axis of the untrawled Eleuterio Canyon. Finally, a CTD transect was conducted in the cross-section between the two submarine canyons on 16 August (Figures1 and S1).

2.3. Field Data Analyses

2.3.1. Mooring Data

Turbidity data acquired during this observational study were processed using *SpikeRemoval* MATLAB (R2023a)'s function [55,56], following (1):

$$[x,\ spikes] = spikeRemoval(w) \tag{1}$$

where w is the input time series, and the outputs are x, which is the de-spiked time series, and *spikes*, which is a structure array that contains the indices of spikes, corresponding values, and replacement values. The complete script and functions can be found in MATLAB's Central File Exchange (https://www.mathworks.com/matlabcentral/fileexchange/69614-spikeremoval [accessed 19 October 2022]).

This function replaces spikes (or outliers) exceeding a threshold value by interpolating among previous and subsequent data points or replacing them with NaN values. The threshold is defined as the mean $\pm$ a given number of standard deviations (std) of windowed data centered at spike locations. In this case, the most suitable threshold was defined as 2 std and 2 passes for detection and replacement of spikes. The turbidimeter at 5 mab presented increasing baseline values over time, indicating the effect of biofouling. Hence, data from this sensor were omitted. Turbidity measurements in FTU could not be converted into estimates of suspended sediment concentration (SSC) since no water samples were collected during the hydrographic survey. Therefore, turbidity values in this paper have been kept as arbitrary units and expressed in FTU.

Current speeds and directions obtained from the 300 kHz ADCP were decomposed into E-W and N-S components. In order to obtain the across- and along-canyon velocity components, the zonal and meridional current components were rotated 25° counterclockwise, so that their reference frames became aligned to the local canyon axis orientation. This rotation converted the X axis values into the across-canyon velocity component (positive towards the SE), and the Y axis values into the along-canyon velocity component (positive down-canyon). Progressive vector diagrams were computed following (2):

$$\sum_{t=0}^{N} \vec{V}(t)\Delta t \tag{2}$$

where the time step used was 5 min, which corresponded to the measuring interval of the 300 kHz ADCP.

Progressive vector diagrams essentially show the cumulative displacement of a particle, such as a water parcel, over time based on velocity data, allowing the understanding

of the dynamics of ocean currents and their time evolution [57]. For the purpose of the present study, they were computed for the depth-cells corresponding to 80 mab, 60 mab, 40 mab, and 20 mab.

2.3.2. CTD Data

Raw CTD data were first converted into engineering units using the Data Conversion function of SBE Data Processing software (v. 7.26.7). Converted CTD data were then filtered using two low-pass filters (0.03 s and 0.15 s, respectively) to eliminate any high-frequency fluctuations. Variables such as salinity, potential density, and potential temperature were derived from primary variables (conductivity, temperature, and pressure). A loop was then applied to remove the effects of the CTD moving up and down the water column with the pitch, roll, and heave of the ship. Any negative pressure changes on the downcast (i.e., CTD moving upwards) or positive pressure changes on the upcast (i.e., CTD moving downwards) were flagged as "bad quality" and were removed. Afterwards, data were binned to 1 m intervals, and visualized using Ocean Data View (ODV) software (v. 5.6.5) [58]. Finally, interpolated plots representing CTD and turbidity data were created using the Data-Interpolating Variational Analysis (DIVA) gridding software [59] included in ODV software (DIVA parameters: scale lengths chosen automatically; quality limit: 3.0; excluding outliers).

2.4. Ancillary Data

2.4.1. Wave Conditions

Wave conditions during the monitoring period were obtained from model data from the "Mediterranean Sea Waves forecasting system (Med-WAV)" model [60]. The Med-WAV consists of a multi-year (1993–2019) wave reanalysis model composed by hourly wave parameters at 1/24° horizontal distribution, covering the Mediterranean Sea and extending up to 18.125° W into the Atlantic Ocean. The wave input parameters, which are available through the CMEMS (Copernicus Marine Environment Monitoring Service) [61], consist of 17 hourly wave parameters validated using wave buoy and satellite measurements.

For the purpose of this study, data were selected and plotted for a particular grid point (latitude: 38°11.4′ N and longitude: 013°25.2′ E) (Figure 1), which was the closest to the mooring site and is a representative location to assess the wave conditions at the study area. Model results included the following parameters: significant wave height (Hs, m), mean wave direction (θ, °), and primary mean wave period (Tp, s).

2.4.2. Fishing Effort

Trawling activity at the Gulf of Palermo was determined from Vessel Monitoring System (VMS) data, a mandatory transmission system since 2005 in all European vessels with an overall length over 15 m [62]. Vessels with VMS transmit information of their position, speed, and heading to the network of the national coastal guard by the Inmarsat-C system, at intervals of 1–2 h. However, VMS data for research and impact assessment have some limitations, including a long duration between position records that can lead to incomplete coverage of vessel activities and a lack of information on whether a vessel is actually fishing or drifting when the position is recorded [63]. To overcome the low sampling frequency, vessel positioning was interpolated based on its speed and heading and accounting for its drift using the R package VMSbase [64]. Trawling intensity, expressed as mean swept area in hectares, was estimated using VMS data from 2008 to 2016 in the Gulf of Palermo in 100 m^2 grid cells [64]. The VMS data allowed us to define the extent of the fishing effort at the Oreto Canyon and its surroundings (Figure 1).

For the purpose of this study, we isolated a grid cell that covered the axis, and the eastern and the western canyon flanks of the Oreto Canyon, where the maximum fishing intensity can be found (Figures1 and S1a). Afterwards, the number of trawlers was calculated using VMS data from 8 August 2016 to 12 January 2017. Then, the number of fishing hauls was isolated from each vessel's trip by removing steaming and non-fishing behaviors (i.e., navigating and drifting), and by considering that bottom trawling was only

carried out while bottom trawlers were going down-canyon at speeds between 0.4 and 5 knots, following the procedure described in [64].

3. Results

3.1. Forcing Conditions

3.1.1. Wave Regime

During the monitoring period, significant wave height (Hs) ranged between 0.1 and 1.7 m during the more quiescent summer months (August and September), and between 0.1 and 3.6 m during fall and winter months (October, November, December, and January) (Figure 2a). From late October to early January, several storms, defined as sustained Hs greater than 2 m for more than 6 h [65], were recorded, the majority of them caused by strong northern and northwesterly winds. Wave mean period (Tp) during storm events varied between 3.2 and 5.9 s (Figure 2b). The maximum Hs and Tp on the Oreto Canyon registered during the mooring deployment were 3.6 m and 5.5 s, respectively, which corresponded to a north-westerly storm that occurred on 6 January 2017 (Figure 2a,b).

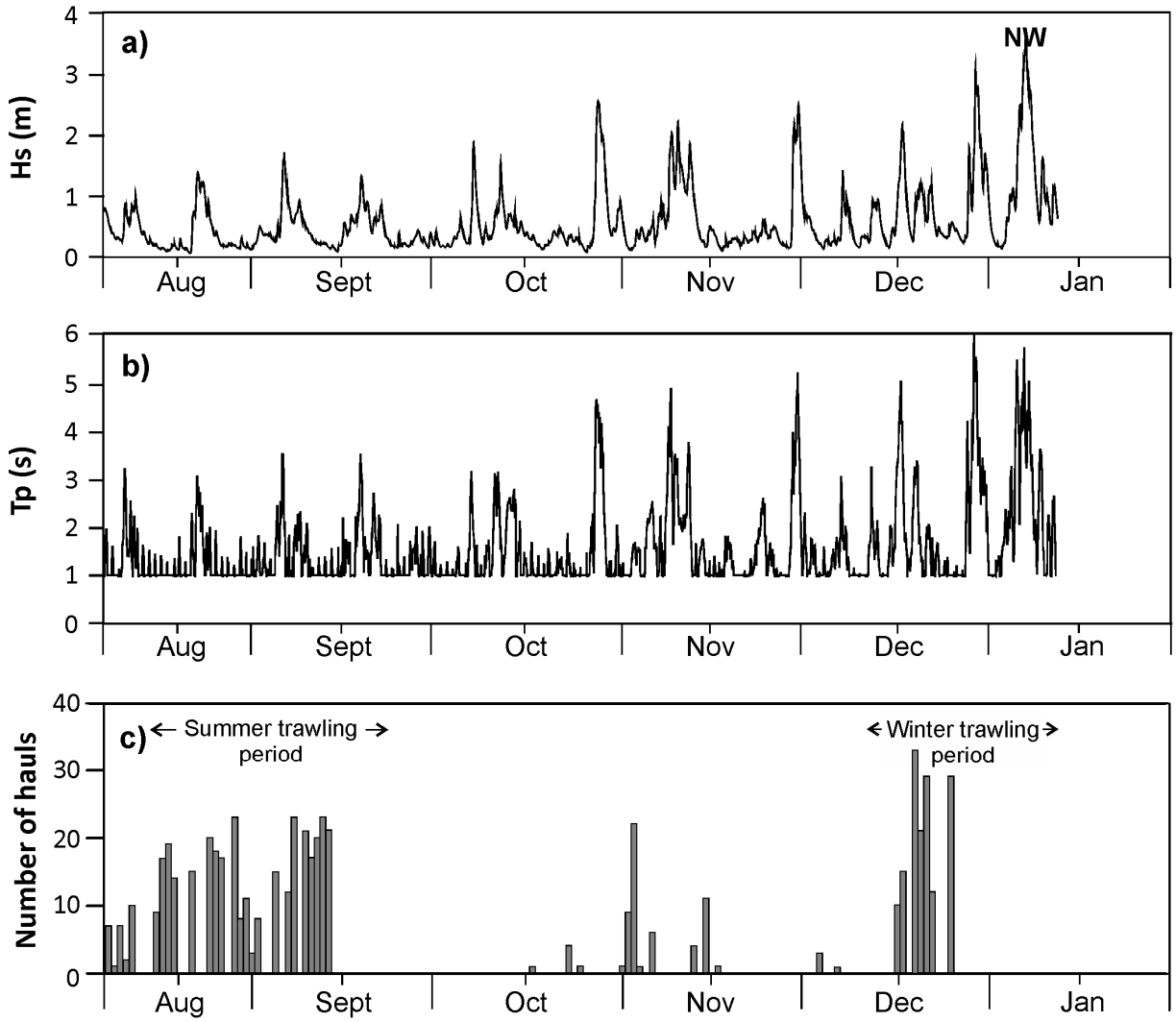

Figure 2. Forcing conditions during the deployment period. (**a**) Significant wave height (Hs), indicating the wave direction of the northwesterly (NW) storm occurring on 6 January 2017, and (**b**) primary wave mean period (Tp, s), obtained from the Med-WAV model. (**c**) Number of daily hauls counted from a grid cell covering the canyon axis, and the eastern and the western canyon flanks of the Oreto Canyon.

3.1.2. Bottom Trawling Activity

The trawl effort during the monitoring period indicated that the most intense trawling activity over the study area took place at the fishing grounds located along the axis of the Oreto Canyon, generally ranging from 250 m to 750 m depth (Figures1 and S1a), and at the fishing ground situated at the upper slope located northwards from Cape Zafferano (Figure 1). The fishing activity at these fishing grounds was principally carried out by eight bottom trawlers registered in Porticello and Palermo harbors.

Trawling effort over these fishing grounds varied throughout the monitoring period (Figures 2c and 3). During August, bottom trawlers were mostly concentrated in the Oreto canyon axis fishing ground (Figures 2c and 3a,b), while there was low to negligible presence of bottom trawlers on the upper slope fishing ground northwards from Cape Zafferano (Figure 3a,b). During the first half of September, the presence of bottom trawlers increased in the upper slope fishing ground, as well as in the Oreto canyon axis fishing ground (Figure 3c), where bottom trawlers performed between 1 to 23 hauls per day (Figure 2c). From mid-September to late-October, bottom trawling activity disappeared in the Oreto canyon axis fishing ground (Figures 2c and 3d–f). Only during the second half of September, bottom trawlers moved to shallower fishing grounds on the continental shelf (Figure 3d).

In November, fishing activity increased again, not only in the Oreto canyon axis fishing ground, where the number of hauls fluctuated between one and twenty-two per day (Figure 2c), but also on the continental shelf's fishing ground and on the upper slope fishing ground northwards from Cape Zafferano (Figure 3g,h). In the first half of December, the presence of bottom trawlers slightly decreased in the Oreto canyon axis fishing ground, increasing again in the second half of December (Figure 3i,j), with one to thirty-three hauls per day (Figure 2c). Finally, in the first half of January, the presence of bottom trawlers decreased in the Oreto canyon axis fishing ground since bottom trawlers had moved again to the upper slope fishing ground northwards from Cape Zafferano (Figures 2c and 3k).

3.2. Hydrographic and Turbidity Structure in Oreto and Eleuterio Canyons

The hydrographic data obtained during the CTD transects conducted along the Oreto and Eleuterio submarine canyons, and in the mid-slope hydrographic section between them, revealed distinct patterns in temperature and salinity throughout the water column ascribed to the different water masses present in the study area (Figures4, S2 and S3). The upper part of the water column was occupied by the Modified Atlantic Water (MAW), characterized near the surface by waters with distinctly low salinities (37.9–38.1) and high temperatures (>15 °C), most probably influenced by the seasonal summer thermocline, and by temperatures between 13.5 and 15 °C and salinity values ranging from 38.1 to 38.6 underneath, reaching water depths down to 200 m (Figures4, S2 and S3). Below, and down to about 700 m water depth, the temperature and salinity values showed the more saline Levantine Intermediate Water (LIW), which is characterized by temperatures ranging from 13 to 15.5 °C and salinities from 38.4 to 39.1 (Figure 4, Figures S2 and S3). The deepest casts (>700 m depth) recorded the Tyrrhenian Deep Water (TDW), which showed temperatures over 12.8 °C and salinity values between 38.5 and 38.7 (Figures4, S2 and S3).

The turbidity vertical profiles obtained by the turbidity sensor attached to the CTD showed the distribution of the nepheloid structure in the water column along the CTD transects (Figure 5). Generally, increases in turbidity were observed near the seafloor and at mid-waters, generating bottom and intermediate nepheloid layers, BNLs and INLs, respectively (Figure 5). In the Oreto Canyon CTD transect, increased turbidity values were observed between 100 and 200 m depth where a BNL developed at the outer shelf and canyon head, showing turbidity values of ~0.2 FTU (Figure 5a; station #1). This layer extended offshore and down-canyon, as observed by the slight turbidity increase in station #2 (Figure 5a). The maximum turbidity values were found down-canyon between 400 and 500 m depth in a BNL, which reached 0.8 FTU (Figures5a and S4a). A detachment of this BNL extended almost 3 km offshore as an INL, which was observed at station #4 at the same water depth, but with decreasing turbidity values between 0.2 and 0.4 FTU

(Figures5a and S4a). The lowest turbidity values (i.e., clear waters) were observed 8.5 km offshore, from the surface down to 1092 m water depth, at the deepest hydrographic station #5 (Figure 5a).

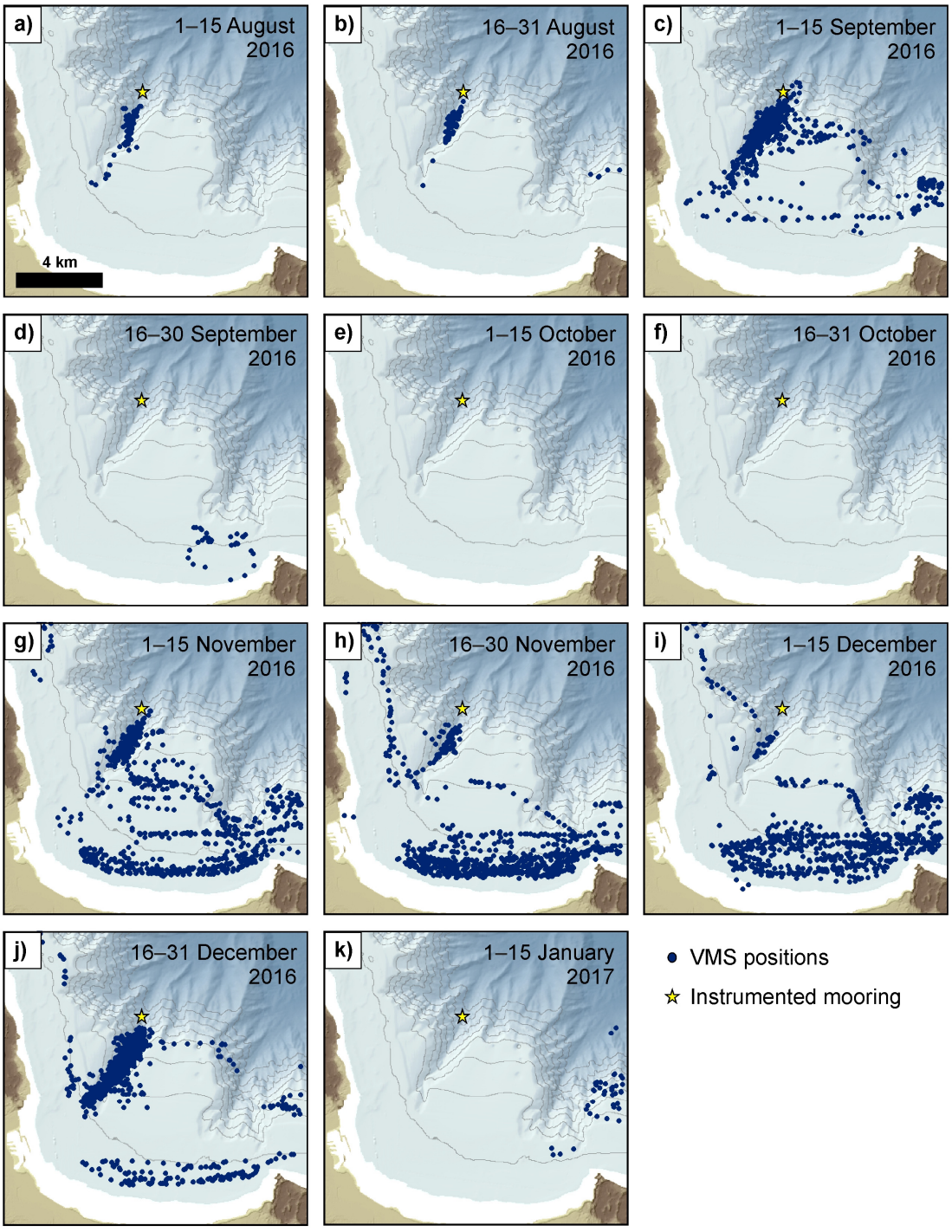

Figure 3. Vessel Monitoring System (VMS) positions of bottom trawlers (blue dots) over the study area during the monitoring period, displayed every 15 days from 1 August 2016 to 15 January 2017. The yellow star indicates the location of the instrumented mooring line.

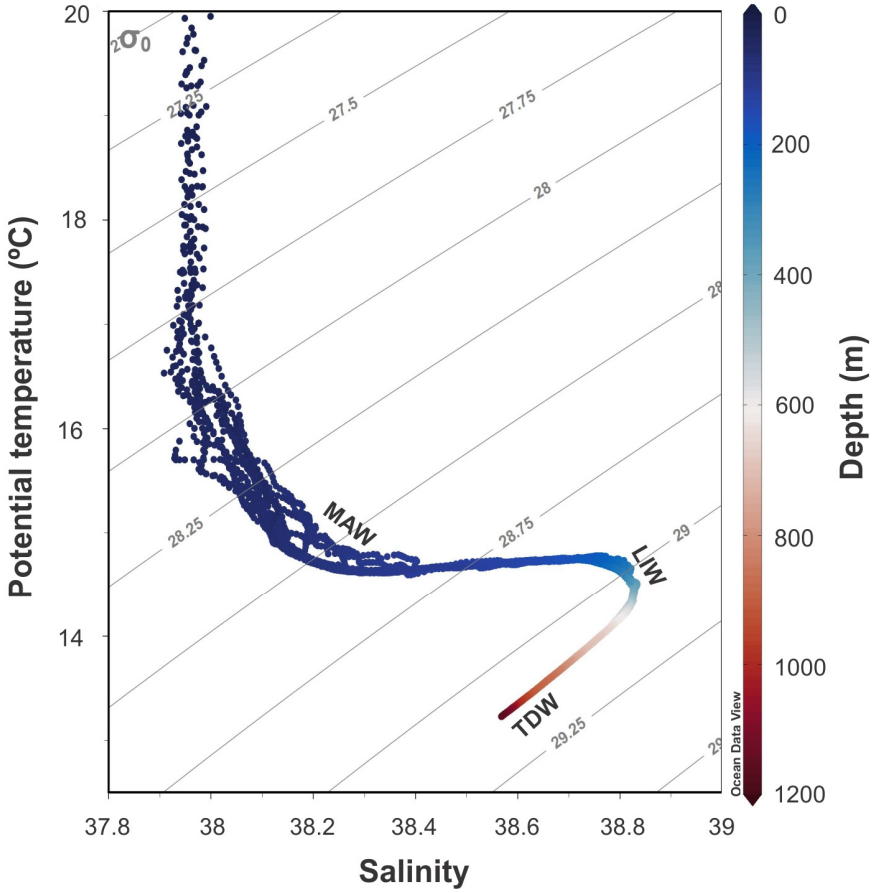

Figure 4. General TS diagram for all the hydrographic casts collected during the CTD transects conducted along the Oreto and Eleuterio submarine canyons, as well as in the mid-slope section between them. The different water masses that can be identified in the study area are the Modified Atlantic Water (MAW), the Levantine Intermediate Water (LIW), and the Tyrrhenian Deep Water (TDW) (data plotted using Ocean Data View v. 5.6.5).

The Eleuterio Canyon CTD transect showed generally lower turbidity values throughout the entire water column (Figure 5b). In this canyon, there were slight increases in turbidity, reaching values of 0.2 FTU, that corresponded to less-developed BNLs and detaching INLs at different water depths (Figure 5b). An INL was observed between 100 and 150 m water depth, at the canyon head, extending 3 km offshore (Figures5b and S4b). Underneath, there was a clearer water layer down to 250 m depth (Figure 5b) and a weak BNL extending down-canyon from 300 to ~600 m water depth (Figures5b and S4b), giving rise to a low concentrated (~0.2 FTU) INL developed at ~400 m depth, stretching offshore for about 3.5 km (Figure 5b; station #9). Similar to the Oreto Canyon, the lowest turbidity values in the Eleuterio Canyon were found at the deepest hydrographic station #10, from the surface down to 1149 m water depth (Figure 5b).

The CTD transect conducted at mid-slope depths between the Oreto and Eleuterio submarine canyons showed clear water from the surface down to ~300 m water depth (Figure 5c) and increasing turbidity values from 300 m to the deepest part of the profiled water column, particularly in the station conducted at the Oreto Canyon (station #3), where turbidity reached 0.8 FTU (Figure 5c). The continental slope between the two submarine canyons (200–300 m depth) also showed, near the bottom, increasing turbidity, peaking at about 0.4 FTU (Figure 5c; station #11).

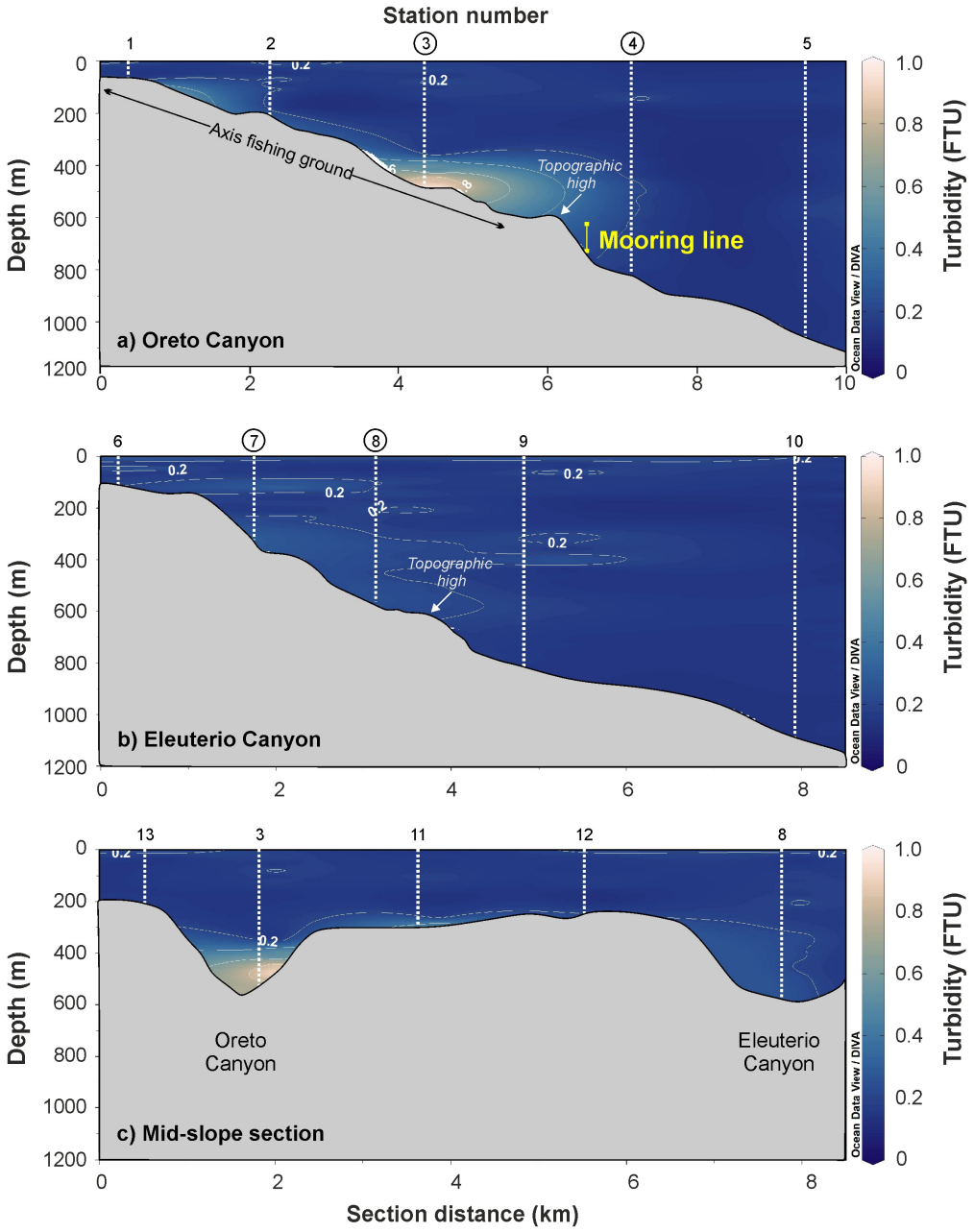

Figure 5. Hydrographic transects conducted during 15 August and 16 August 2016, showing the spatial distribution of water turbidity, in Formazin Turbidity Units (FTU), throughout the water column along (**a**) the Oreto Canyon and (**b**) the Eleuterio Canyon, and (**c**) in the mid-slope section between the two submarine canyons (see transects in Figure 1). The yellow vertical line in panel (**a**) indicates the relative location, water depth, and length of the instrumented mooring line deployed in the axis of the Oreto Canyon. The black arrow in panel (**a**) indicates the approximate location of the canyon axis fishing ground within Oreto Canyon (data plotted using Ocean Data View v. 5.6.5). Circled CTD casts indicate vertical turbidity profiles that were examined (an example is provided in Figure S4 to show the details in these profiles).

3.3. Time Series of Temperature, Currents, and Turbidity in the Oreto Canyon

The temperature time series, recorded by the turbidimeters placed along the mooring line, showed values ranging between 13.5 and 14.5 °C throughout the deployment period (Figure 6a). Notably, there was a difference of approximately 0.25 °C between the turbidimeter placed at 80 mab (at 670 m water depth) and the turbidimeter placed at 10 mab (at 740 m water depth) (Figure 6a). The highest recorded temperature occurred

on December 22, 2016, while the lowest temperature was observed on January 10, 2017 (Figure 6a).

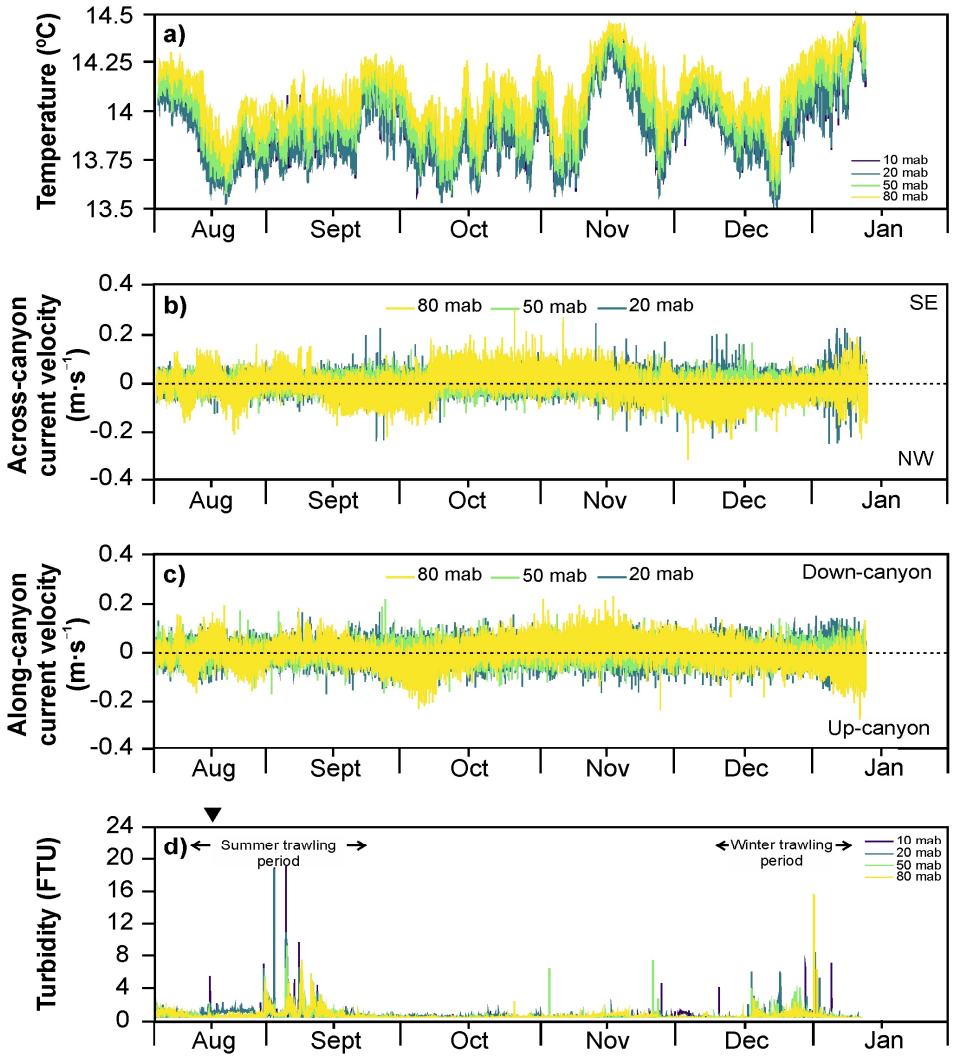

Figure 6. Time series of (**a**) temperature (°C), (**b**) across-canyon current velocity ($m \cdot s^{-1}$), (**c**) along-canyon current velocity ($m \cdot s^{-1}$), and (**d**) turbidity (FTU) measured by the different sensors installed along the instrumented mooring line deployed in the axis of Oreto Canyon. Current velocities below 20 mab are not displayed for both across-canyon (**b**) and along-canyon (**c**) components due to the presence of highly noisy data. The inverted black triangle in panel (**d**) indicates the time when the CTD transects were conducted.

Current velocities during most of the deployment period ranged between 0.1 and 0.2 $m \cdot s^{-1}$ in both across- and along-canyon directions (Figure 6b,c). However, there were instances of increased current velocities exceeding 0.3 $m \cdot s^{-1}$ during the fall and winter months (Figure 6b,c). The analyses of time series showed that currents and temperature were mostly dominated by near-inertial motions (~18h). The inertial motions, defined by the Coriolis parameter (f), which depends on the rotation of the Earth ($\Omega = 7.292 \cdot 10^{-5}$ s) and the latitude (φ), were calculated at the study area ($\varphi = 38.2$ °N) following the equation $f = 2\,\Omega \sin \varphi$, and resulted in a periodicity of 19.4 h.

The variations in current velocity also exhibited distinct patterns depending on the height above the bottom, as evidenced by the progressive vector diagrams of the currents (Figure 7). Starting on 7 August and for the first 15 days, currents at 80 mab were relatively confined, with small displacements in both along- and across-canyon directions of ~2 km (Figure 7a). From 22 September, the currents at 80 mab became relatively unconfined,

showing minimal influence from the canyon topography (Figure 7a). During this period, the currents flowed preferentially towards the northwest until 26 September, when they gradually shifted towards the southeast and predominantly up-canyon (Figure 7a). Conversely, currents below 80 mab were relatively confined due to the influence of the canyon topography and were predominantly oriented along the canyon axis with a significant up-canyon component (Figure 7b,c). On 23 October, a turn in the current direction affected all depths. Currents at 80 mab progressively turned down-canyon, maintaining the elliptical pattern, and afterwards gradually shifted towards the northwest (Figure 7a). In contrast, currents closer to the bottom flowed down-canyon homogeneously through the sampled water column until 3 November (Figure 7b–d). Afterwards, currents at 60 and 40 mab shifted, flowing preferentially along the axis with a predominant up-canyon component, while still being affected by current oscillations directed down-canyon (Figure 7b,c). This pattern was also described by currents close to the bottom (20 mab) (Figure 7d). However, the down-canyon component seemed more relevant, with progressive vectors indicating a gradual shift of the currents towards the southeast (Figure 7d).

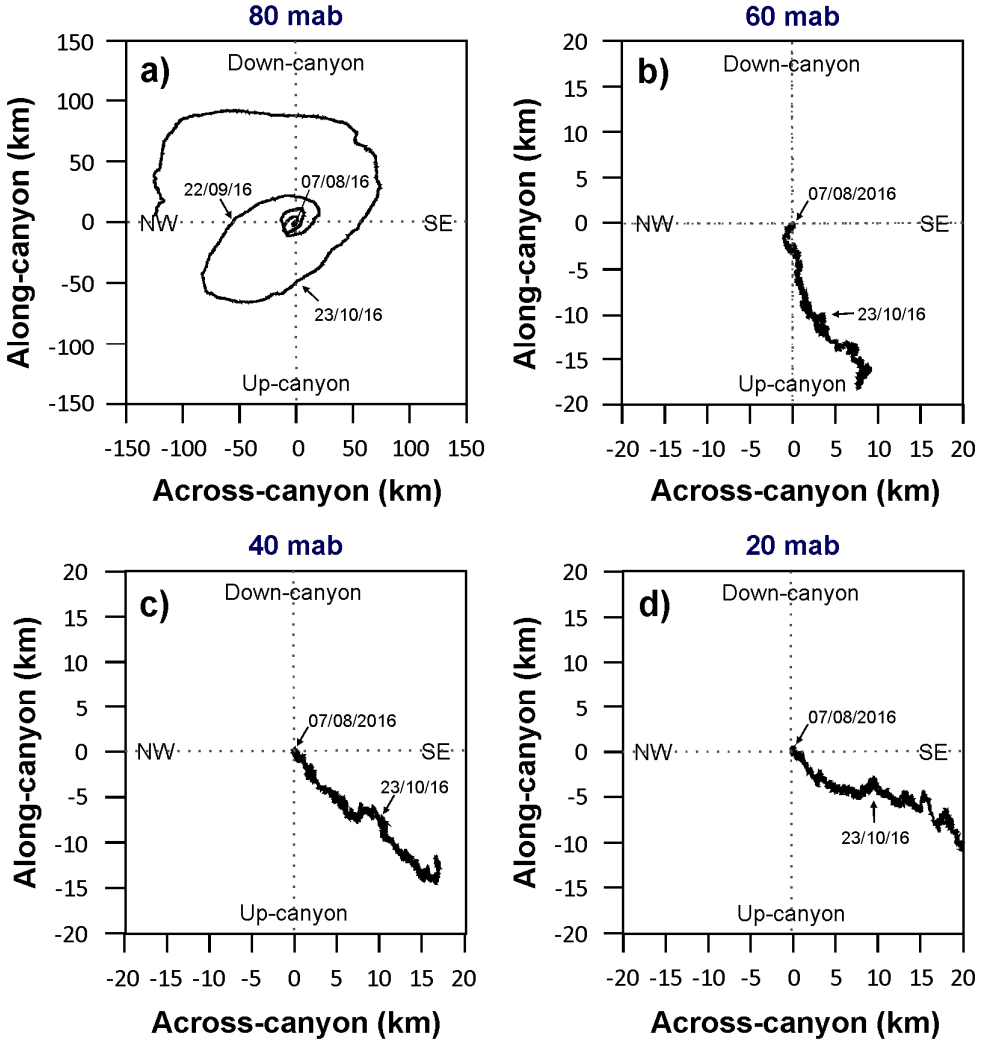

Figure 7. (**a**–**d**) Progressive vector diagrams computed from 4 levels of water currents (80, 60, 40, and 20 mab) obtained by the downward-looking 300 kHz Acoustic Doppler Current Profiler (ADCP) installed in the instrumented mooring line with a 5 min measuring interval during the monitoring period. Starting points are (0, 0) for all the diagrams. Horizontal and vertical axes are across-canyon and along-canyon components, respectively, expressed in km. Note the change in scale in panel (**a**) in both horizontal and vertical axes.

The turbidity record displayed baseline values for the majority of the deployment period, characterized by turbidity shifts ranging from 1 to 3 FTU throughout the monitored water column. However, there were two distinct periods of elevated turbidity, occurring from mid-August to mid-September and from mid-December to early January (Figure 6d), that coincided with the most intense bottom trawling periods during the deployment (Figure 2c). During the summer period, several turbidity peaks, ranging from 4 to 7 FTU, were observed across all depths (10–80 mab), with exceptional higher near-bottom turbidity peaks of approximately 20 FTU recorded in early September (Figure 6d). Subsequently, between the transition from summer to winter, water turbidity gradually decreased and remained within baseline values, typically fluctuating between 1 and 3 FTU. Nevertheless, sporadic turbidity peaks of 8 FTU were recorded at 20 mab in early and late November. Increased turbidity was noted from mid-December to early January, showing peaks from 6 to 8 FTU between 10 and 50 mab, and from 1 to 4 FTU at 80 mab (Figure 6d).

4. Discussion

4.1. Role of Bottom Trawling as a Contemporary Mechanism of Sediment Resuspension

During the present study, the time series of turbidity in the Oreto canyon axis revealed the occurrence of high-concentration turbidity peaks exceeding 2 FTU at <80 m above the seafloor (Figure 6d). These turbidity peaks could not be attributed to natural environmental factors, since no river floods or significant storm events occurred within the study area during the duration of the deployment (Figure 2a,b). However, these turbidity peaks could be related to sediment resuspension caused by bottom trawling activities, as observed by the temporal distribution of these peaks in coincidence with periods of intense trawling activity at the Oreto canyon axis fishing ground (Figures 2c and 6d). This was particularly evident during late August and the first half of September, after the conclusion of the summer holiday period, as well as during the second half of December, coinciding with the Christmas season, when relatively high turbidity increases of 4–7 FTU and 6–8 FTU, respectively, were recorded at all instrumented water depths throughout the water column (Figure 6d). Conversely, lower turbidity values were consistently observed throughout the water column during the bottom trawling intermission at the Oreto canyon axis fishing ground, which occurred in late September and October (Figure 6d). It is likely that during this period, the large bottom trawlers from Palermo and Porticello harbors, which regularly operate in the Oreto Canyon, had relocated to shallower depths of the continental shelf or to alternative fishing grounds situated along the northwestern Sicilian continental margin (Figure 3d–f). Even in periods characterized by relatively low bottom trawling activity in the Oreto Canyon, such as the month of November (Figure 2c), a few isolated high-turbidity peaks were still recorded (Figure 6d). For instance, in early November, these turbidity peaks coincided with isolated bottom trawling activities at the Oreto canyon axis fishing ground (Figure 2c). However, in late November, isolated turbidity peaks occurred on days when bottom trawlers were not in operation (Figures 2c and 6d), which could be the result of a sediment destabilization originating from the Oreto canyon flanks.

These findings in Oreto Canyon support the idea that sediment resuspension induced by bottom trawling activities plays a substantial role in increasing turbidity levels in the water column within submarine canyon environments. Previous studies have effectively demonstrated that the action of bottom trawling gears scraping and ploughing the seabed results in increased near-bottom water turbidity owing to sediment resuspension. After sediment is resuspended by bottom trawlers, the fishing grounds become eroded, potentially leading to preferential re-deposition of coarser sediment fractions [13,66], whereas finer particles are transported by ambient currents towards deeper regions, either as enhanced nepheloid layers [13,22–24,67] or as sediment gravity flows [18–20]. In the context of the Oreto Canyon, the occurrence of sediment gravity flows, characterized by downslope water movement due to the contribution of suspended sediment load to fluid density, was ruled out, since no concurrent increases in current velocity were recorded in the moored instruments when turbidity levels rose (Figure 6). Such sediment gravity flows have been

previously documented in the NW Mediterranean Sea, particularly at the confluence of a trawled tributary valley (Montgrí) with the Palamós canyon axis [13,18]. In that region, trawling-induced resuspended sediments from a canyon flank fishing ground were channelled through the Mongrí tributary, causing significant turbidity peaks coinciding with velocity increases. However, the data collected in our study did not show evidence of these fast sediment gravity flow events channelized through the main axis of the Oreto Canyon. Instead, the moored instruments appeared to intercept the less dense resuspended particles transported by fluctuating currents with relatively low velocities (<0.2 $m \cdot s^{-1}$) confined within the canyon, which reached the mooring instruments with variable temporal offsets relative to the passage of bottom trawlers (Figure 6d). Most likely, these resuspended particles contributed to feeding intermediate and bottom nepheloid layers, which maintained elevated turbidity levels in the water column even some time after the cessation of bottom trawling activities (Figure 6d). This was observed in both the moored instruments and hydrographic profiles conducted within the Oreto Canyon during the ISLAND Cruise, a day after the passage of bottom trawlers (Figures 5a and 6d).

4.2. Role of Water Masses and Current Variability as a Mechanism of Suspended Sediment Transport

The time series of data collected at the Oreto canyon axis during periods of intense trawling activity revealed a consistent pattern where turbidity values typically increased over periods of 2–5 days, in agreement with the low-frequency oscillations of water temperature, and apparently unrelated to variations in the currents (Figures 8 and 9). These oscillations are likely influenced by the presence of mesoscale oceanographic structures affecting the circulation over the Gulf of Palermo continental slope area [45]. Such low-frequency oscillations are ubiquitous in the northwestern Mediterranean Sea, as in the Ligurian Sea or in the Gulf of Lions, and have been associated with the influence of topographic waves (e.g., [68–72]). In continental shelf environments, the passage of topographic waves has been suggested as a controlling mechanism for the cross-shelf exchange of water, sediments, and nutrients [73]. In the Adriatic Sea, for instance, topographic waves triggered by the inflow of a dense water vein were observed propagating along the continental slope with a periodicity of 2–4 days [73]. In the Ligurian Sea, they have been observed along the slope with periods of 10–20 days and across the slope with periods of 3–6 days [74].

Variations in temperature and turbidity at the monitored depths also provided evidence of the oscillation of the interface between the Levantine Intermediate Water (LIW) and the Tyrrhenian Deep Water (TDW). In general, lower turbidity values were observed when the moored instruments recorded relatively cooler temperatures from the TDW, while residual currents flowed preferentially up-canyon (Figures 8 and 9). In contrast, higher turbidity values were recorded during periods characterized by the presence of relatively warmer waters from the LIW at the mooring site, while residual currents flowed preferentially down-canyon (Figures 8 and 9). This most probably suggests that, during active trawling periods within the Oreto canyon axis fishing ground, resuspended sediment particles tend to be retained within the density gradient between the LIW and the TDW. These particles are then likely detached along the isopycnals and transported towards deeper regions of the Oreto Canyon during periods when currents are preferentially down-canyon, ultimately reaching the mooring location (Figures 8 and 9). These results resemble previous findings in the Gulf of Valencia continental slope by [75], which attributed the presence of high turbidity values in intermediate and bottom nepheloid layers to internal waves propagating along the interface between the LIW and the Western Mediterranean Deep Water (WMDW). The resuspended particles from the slope would be maintained in suspension by the existing density gradient between these water masses. Numerous other studies have also related the presence of nepheloid layers with internal waves in various regions (e.g., [76,77]).

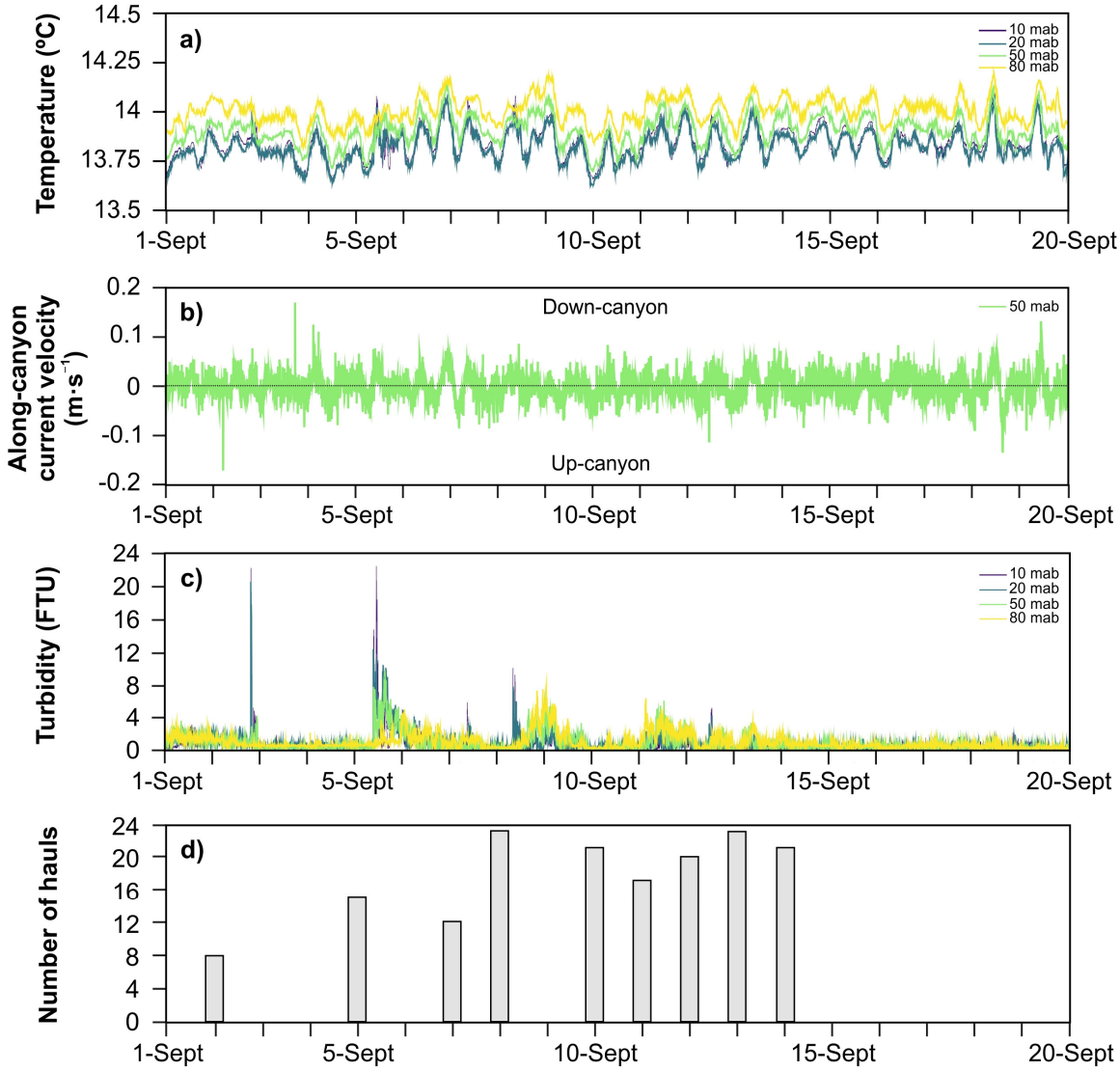

Figure 8. Time series during a highly active trawling period in summer, showing data of (**a**) temperature (°C), (**b**) along-canyon current velocity ($m \cdot s^{-1}$), and (**c**) turbidity (FTU) measured by the different sensors installed along the instrumented mooring line deployed in the axis of Oreto Canyon. (**d**) Number of daily hauls counted from a grid cell covering the canyon axis, and the eastern and the western flanks of the Oreto Canyon from 1 September to 20 September 2016.

Nonetheless, it is worth noting that after a few days of active bottom trawling activity, lower turbidity values could also be recorded in the near-bottom water column monitored by the moored instruments (Figures 8 and 9). This was the case in mid-September (12–14), when the high number of computed trawling hauls did not correspond to significant increases in turbidity values. This suggests that during this period of intense trawling activity at the canyon, the moored instruments did not directly capture the resuspended plume generated immediately after the passage of trawlers. The analyzed VMS data showed an increased number of vessel positions along the Oreto canyon axis, but predominantly located shallower than the mooring location (Figure 5a). The topographic high located at 750 m depth in the canyon axis may in fact act as a natural obstacle preventing the expansion of trawling grounds to deeper depths [78] (Figures5a and S1b), but also act as a ramp to facilitate the detachment of INLs down-canyon. This suggests that the resuspended particles may have already been detached as INLs at shallower depths, which would have

been afterwards advected over the mooring line as diluted INLs, therefore being unnoticed by the moored sensors (Figure 8).

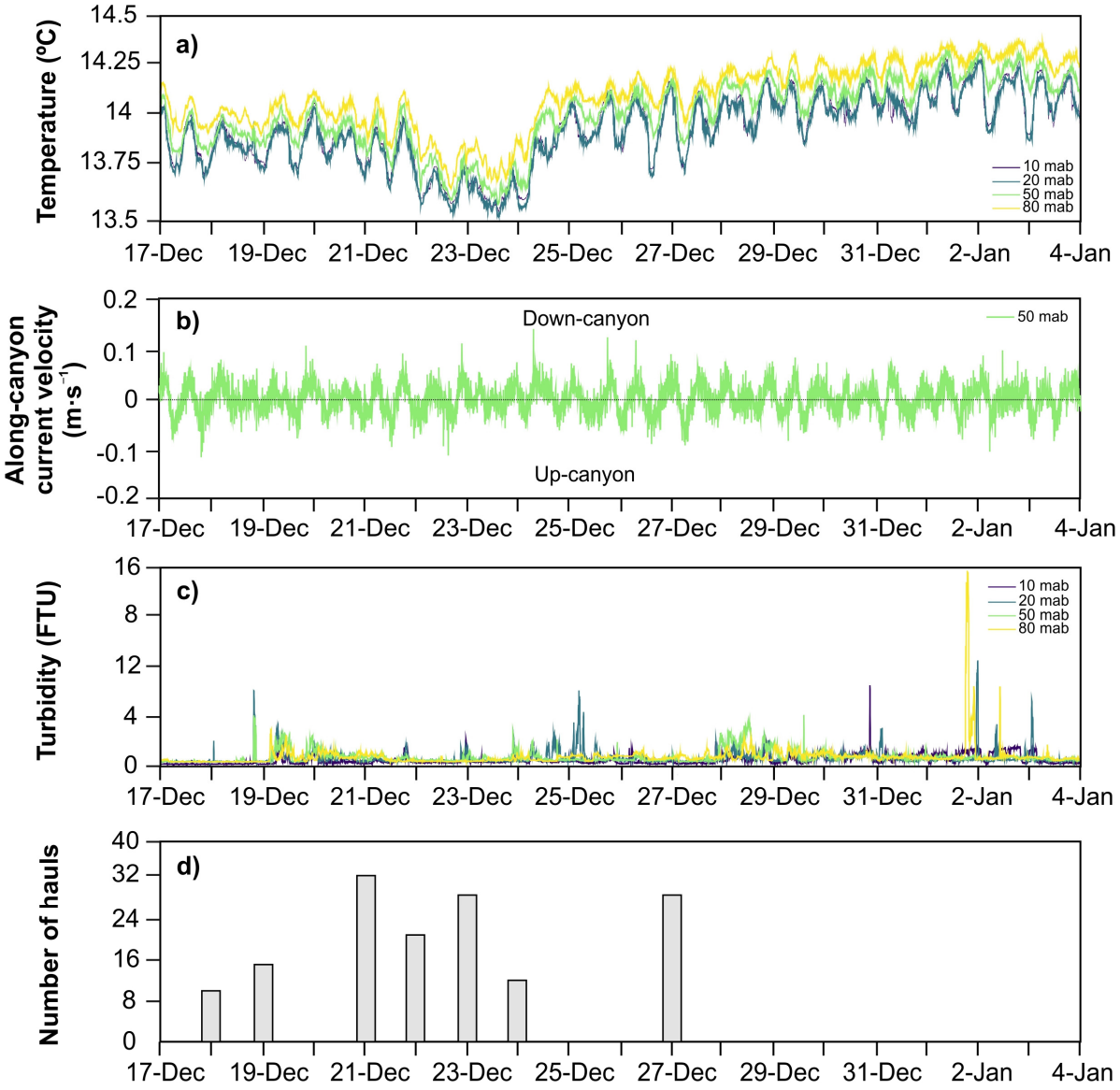

Figure 9. Time series during a highly active trawling period in winter, showing data of (**a**) temperature (°C), (**b**) along-canyon current velocity ($m \cdot s^{-1}$), and (**c**) turbidity (FTU) measured by the different sensors installed along the instrumented mooring line deployed in the axis of Oreto Canyon. (**d**) Number of daily hauls counted from a grid cell covering the canyon axis, and the eastern and the western flanks of the Oreto Canyon from 17 December 2016, to 4 January 2017.

Looking into the details of periods with high turbidity records, it can be seen that overlying the above-described fluctuations associated with topographic waves, fluctuating up- and down-canyon currents were also influenced by the local near-inertial frequency, which had a periodicity of ~18h and modulated the high-frequency oscillations of both temperature and turbidity (Figures 8 and 9).

This behavior was particularly evident during two notable intervals: between 12 September and 15 September 2016, and between 19 December and 22 December 2016 (Figures 10 and 11). For instance, around midday on September 12, the near-bottom instruments (positioned between 10 and 20 mab) recorded a sharp turbidity peak of ~5 FTU, which persisted for approximately 2 h. In contrast, the instruments located at mid-waters (50–80 mab) did not

register such a significant turbidity increase (Figure 10c). Instead, they recorded the subsequent arrival of a less concentrated intermediate nepheloid layer (2–3 FTU) that persisted for several hours, coinciding with a period when currents were primarily directed down-canyon and the temperature values progressively increased (Figure 10). During periods when currents shifted up-canyon and temperature decreased, clear waters were observed. Afterwards, the nepheloid layers were recorded again by the moored instruments on 13 September and 14 September, corresponding to the subsequent two down-canyon inertial cycles (Figure 10). Similarly, during the winter trawling period, from 19 December to 21 December, the turbidity records also displayed fluctuations at near-inertial frequencies, showing analogous behavior. Turbidity levels increased during periods when temperatures rose and currents were directed down-canyon, while turbidity decreased when temperature dropped, and currents were directed up-canyon (Figure 11).

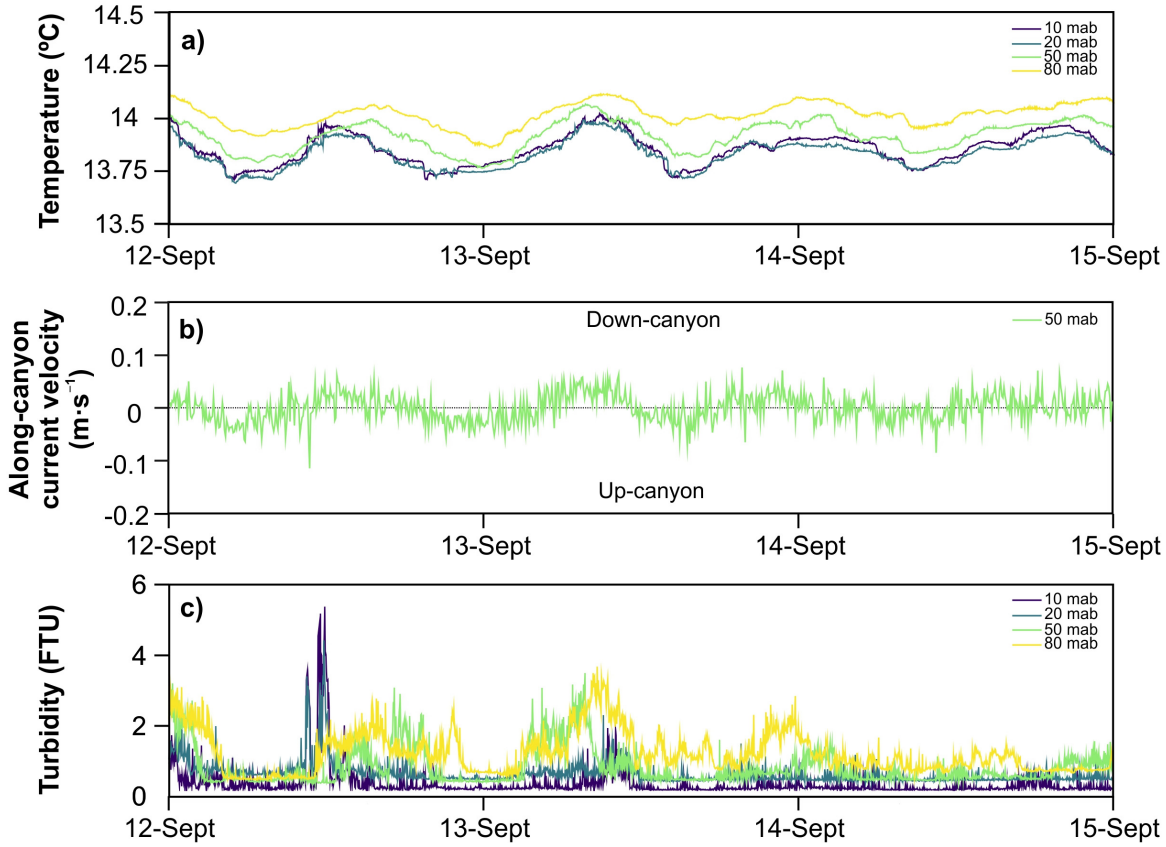

Figure 10. Evolution of (**a**) temperature (°C), (**b**) along-canyon current velocity ($m \cdot s^{-1}$), and (**c**) turbidity (FTU) records measured by the different sensors installed along the instrumented mooring line deployed in Oreto Canyon during a chosen period in summer (12 September to 15 September 2016), showing in detail the oscillation of the monitored parameters at the near-inertial frequency.

The above-described oscillations at near-inertial frequencies are similar to previously reported findings across the Mediterranean Sea (e.g., [72,79]), where near-inertial temperature variations were mainly correlated with along- and across-slope oscillations that modulated the sediment flux direction. It has been postulated that inertial motions are generally generated by atmospheric disturbances, although enhanced near-inertial energy can be found at greater depths in the water column [79]. They can be transported downwards into the ocean by propagating waves that can pass through both stratified and mixed water layers [79]. Some studies, such as [80,81], have suggested that propagating waves interacting with the bottom of continental slopes can cause sediment resuspension. However, turbidity records at the Oreto canyon axis showed no sharp resuspension peaks linked to the near-inertial waves at the canyon. Despite this, currents at near-inertial frequencies

were found to modulate along-canyon sediment fluxes, following the current fluctuations at the same near-inertial time scales (Figures 10 and 11). These findings suggest that currents at near-inertial frequencies did not induce sediment resuspension, but rather they were crucial in advecting sediment resuspended by bottom trawlers along the canyon.

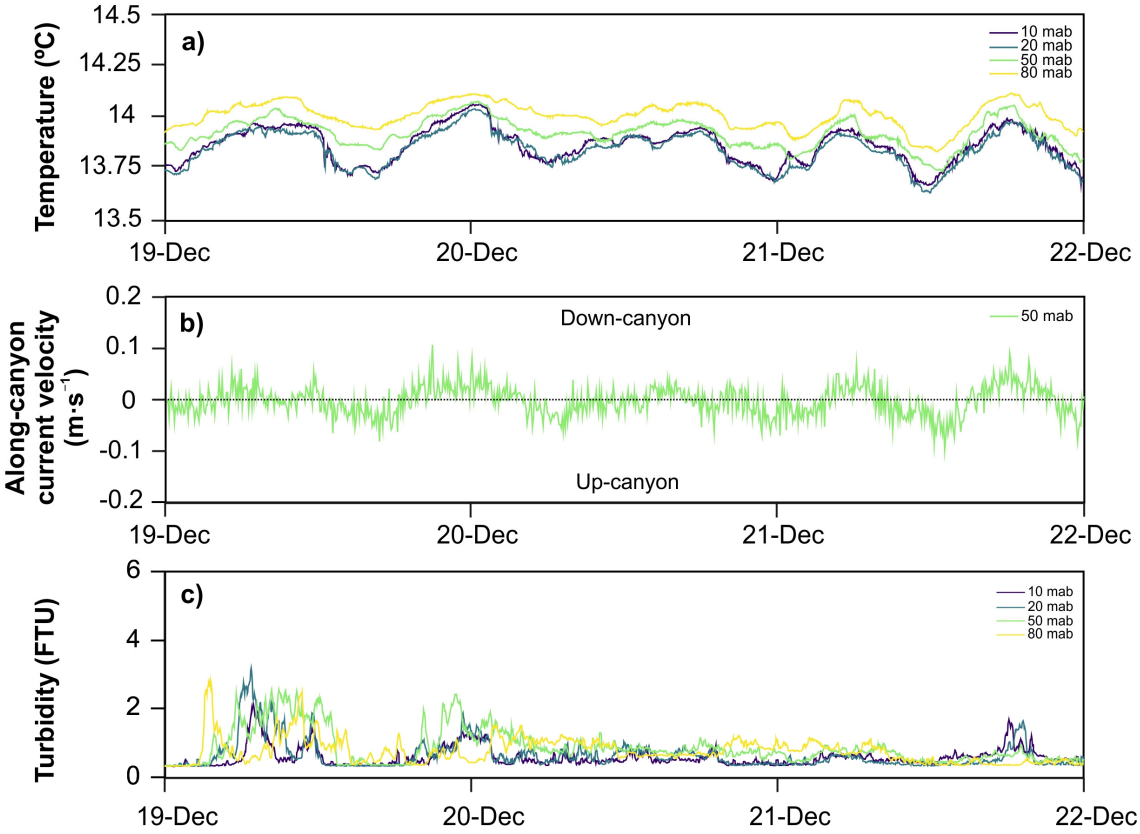

Figure 11. Evolution of (**a**) temperature (°C), (**b**) along-canyon current velocity ($m \cdot s^{-1}$), and (**c**) turbidity (FTU) records measured by the different sensors installed along the instrumented mooring line deployed in Oreto Canyon during a chosen period in winter (19 December to 22 December 2016), showing in detail the oscillation of the monitored parameters at the near-inertial frequency.

Therefore, topographic waves passing over the Gulf of Palermo might exert an important role in controlling sediment transport processes within the Oreto Canyon, favoring the dispersion and transport of sediment particles resuspended from fishing grounds towards deeper parts of the canyon. This mechanism, added to the slow (<0.2 $m \cdot s^{-1}$) and oscillating up-/down-canyon near-inertial flow (Figures 10 and 11), ultimately governs the distribution and fate of trawling-induced resuspended particles, which may either reach the deeper parts of the canyon where the mooring was located or settle before along the canyon axis. This sediment transport mechanism within the Oreto Canyon may also help explain the elevated sedimentation rates reported in the canyon axis [32,33]. These rates have increased from 0.11 to 0.73 $cm \cdot yr^{-1}$ at ~500 m depth and from 0.11 to 0.21 $cm \cdot yr^{-1}$ at ~800 m depth within the canyon axis after the industrialization of bottom trawling fleets during the 1980s [32].

Similar increases in sedimentation rates attributed to bottom trawling activities since the 1980s have been documented in the neighboring Eleuterio and Arenella submarine canyons, both at around ~500 m depth. In these canyons, sedimentation rates have increased from 0.11 to 1.38 $cm \cdot yr^{-1}$ and from 0.13 to 1.37 $cm \cdot yr^{-1}$, respectively, in the mid-1980s [32]. In fact, both canyons can intercept the sediment supplied to and resuspended in the outer shelf and mid-slope by bottom trawling activities (Figures 1 and 3), which can then be transported by the along-margin Tyrrhenian Sicilian Current (TSC) to

the head and axis of these canyons [31]. Although we did not record turbidity time series in any of these canyons, CTD turbidity data in Eleuterio Canyon suggests the potential impact of trawling-derived resuspended sediment at the canyon head (Figure 5b).

Overall, our results support the idea that trawling-induced resuspension has a significant role in increasing turbidity levels within the Oreto Canyon, with a varying intensity that depends on the position of trawlers within the canyon, as well as the prevailing hydrodynamics, which ultimately control the transport and the fate of resuspended particles.

5. Conclusions

This study provides new insights about the nepheloid layer distribution in the Oreto and Eleuterio submarine canyons and the potential mechanisms contributing to the sediment resuspension and advection in these submarine canyons. In the Oreto Canyon, bottom trawling activities were identified as the primary mechanism of sediment resuspension and generation of nepheloid layers. The time series analyses conducted in the lower reaches of this canyon showed that turbidity values generally increased during the most active trawling periods, exhibiting periodic oscillation over about 2–5 days, in agreement with the low-frequency oscillations of water temperature, and unrelated to variations in the currents. These temperature oscillations appeared to be related to the oscillation of the interface between the LIW and the TDW, which were likely influenced by the passage of topographic waves over the area. These waves, combined with the slow (<0.2 $m \cdot s^{-1}$) and oscillating near-inertial (~18 h) currents, determined the distribution, transport, and fate of trawling-induced resuspended sediments, advecting turbid water down-canyon. This study also presents findings that the alterations in water turbidity and nepheloid layer structure by bottom trawling activities occur not only in the NW Mediterranean, where it was documented until now, but also in other Mediterranean margins.

In summary, the present paper confirms that the resuspension capability of bottom trawlers can alter the sedimentary dynamics of submarine canyons affected by this human activity and highlights the importance of understanding the role of the hydrodynamics prevailing within submarine canyon environments in the dispersal and transport of suspended sediment particles. Further research is needed to comprehensively assess the impacts resulting from this human activity in deep-sea environments.

Supplementary Materials: The following supporting information can be downloaded at: https://www.mdpi.com/article/10.3390/jmse12071050/s1. Figure S1: Bathymetric map of the Oreto Canyon, showing the location of the instrumented mooring line (yellow star) and the CTD stations sampled (grey dots) around the canyon. The overlying density raster represents the mean annual trawling intensity as swept area per year obtained from Vessel Monitoring System (VMS) data between 2008 and 2016. Bathymetric contour lines are displayed every 50 m. The black dashed lines correspond to the (b) along-canyon and (c) across-canyon sections showing the location of the instrumented mooring line (not scaled). In panels (b) and (c), the black arrows indicate the approximate location of the axial and slope fishing grounds in Oreto Canyon, respectively. Figure S2: Hydrographic transect conducted during 15 August and 16 August 2016, showing the spatial distribution of (a) potential temperature (°C) and (b) salinity, throughout the water column along the Oreto Canyon (see transect in Figure 1). The yellow vertical line indicates the relative location, water depth, and length of the instrumented mooring line deployed in the axis of the Oreto Canyon. The black arrow indicates the approximate location of the canyon axis fishing ground within Oreto Canyon (data plotted using Ocean Data View v. 5.6.5). Figure S3: Hydrographic transect conducted during 16 August 2016, showing the spatial distribution of (a) potential temperature (°C) and (b) salinity, throughout the water column along the Eleuterio Canyon (see transect in Figure 1) (data plotted using Ocean Data View v. 5.6.5). Figure S4: Example of vertical turbidity profiles from selected CTD stations in (a) Oreto and (b) Eleuterio Canyons. See Figure 5 for profiling location along the different sections.

Author Contributions: Conceptualization, C.L.I. and P.P.; Methodology: C.L.I. and P.P.; Data curation: M.A.-C. and T.R.; Formal analysis, M.A.-C., C.L.I. and T.R.; Visualization, M.A.-C.; Resources, C.L.I., P.P. and A.P.; Writing—original draft, M.A.-C., Writing—review and editing, C.L.I., P.P., T.R. and A.P. All authors have read and agreed to the published version of the manuscript.

Funding: The results presented in this paper were obtained during the Exploring Sicilian Canyon Dynamics (ISLAND) Project, supported by the European Commission, Seventh Framework Eurofleets-2 Program (grant no. 312762). This work was also supported by the "Assessment of Bottom-trawling Impacts in Deep-sea Sediments" (ABIDES) Spanish Research Project (CTM2015-65142-R, Spanish Ministry of Economy and Competitiveness) and by the "Assessment of Bottom-trawling impacts in deep benthic Communities" (ABRIC) Spanish Research Project (RTI2018-096434-B-100, Spanish Ministry of Science, Innovation, and Universities). This work contributes to ICM-CSIC's "Center of Excellence" Severo Ochoa (CEX2019-000928, Spanish Ministry of Science, Innovation, and Universities). Finally, we acknowledge the H2020 MSC Action IF CAR HABISS (GA890815, European Commission). MA-C, CL, PP and AP belonging to the Consolidated Research Group on Littoral and Oceanic Processes, supported by grant 2021 SGR 663 (Generalitat de Catalunya). MA-C is funded by the "Margarita Salas" postdoctoral research grant from the Spanish Ministry of Universities.

Institutional Review Board Statement: Not applicable.

Informed Consent Statement: Not applicable.

Data Availability Statement: The raw data supporting the conclusions of this article will be made available by the authors on request.

Acknowledgments: We would like to thank the crew of R/V *Ángeles Alvariño* and the ISLAND cruise team for their guidance and assistance during the experimental work, as well as Jose Pozo and Maribel Lloret for their assistance in the preparation and deployment of the instrumented mooring line. We extend our gratitude to Antonia Sciabica and Bianca Colmone for providing their sailboat *Viva* to retrieve the mooring line, and to Attilio Sulli and Mauro Agate (University of Palermo) for their logistic support.

Conflicts of Interest: The authors declare no conflicts of interest.

References

1. Harris, P.T.; Whiteway, T. Global distribution of large submarine canyons: Geomorphic differences between active and passive continental margins. *Mar. Geol.* **2011**, *285*, 69–86. [CrossRef]
2. Allen, S.E.; Durrieu de Madron, X. A review of the role of submarine canyons in deep-ocean exchange with the shelf. *Ocean Sci.* **2009**, *5*, 607–620. [CrossRef]
3. De Stigter, H.C.; Jesus, C.C.; Boer, W.; Richter, T.O.; Costa, A.; van Weering, T.C. Recent sediment transport and deposition in the Lisbon-Setúbal and Cascais submarine canyons, Portuguese continental margin. *Deep Sea Res. Part II Top. Stud. Oceanogr.* **2011**, *58*, 2321–2344. [CrossRef]
4. Talling, P.J. On the triggers, resulting flow types and frequencies of subaqueous sediment density flows in different settings. *Mar. Geol.* **2014**, *352*, 155–182. [CrossRef]
5. Puig, P.; Palanques, A.; Martín, J. Contemporary sediment-transport processes in submarine canyons. *Annu. Rev. Mar. Sci.* **2014**, *6*, 53–77. [CrossRef] [PubMed]
6. Porter, M.; Inall, M.E.; Hopkins, J.; Palmer, M.R.; Dale, A.C.; Aleynik, D.; Barth, J.A.; Mahaffey, C.; Smeed, D.A. Glider observations of enhanced deep water upwelling at a shelf break canyon: A mechanism for cross-slope carbon and nutrient exchange. *J. Geophys. Res. Ocean.* **2016**, *121*, 7575–7588. [CrossRef]
7. De Leo, F.C.; Smith, C.R.; Rowden, A.A.; Bowden, D.A.; Clark, M.R. Submarine canyons: Hotspots of benthic biomass and productivity in the deep sea. *Proc. R. Soc. B Biol. Sci.* **2010**, *277*, 2783–2792. [CrossRef] [PubMed]
8. De Leo, F.C.; Vetter, E.W.; Smith, C.R.; Rowden, A.A.; McGranaghan, M. Spatial scale-dependent habitat heterogeneity influences submarine canyon macrofaunal abundance and diversity off the Main and Northwest Hawaiian Islands. *Deep Sea Res. Part II Top. Stud. Oceanogr.* **2014**, *104*, 267–290. [CrossRef]
9. Vetter, E.W.; Smith, C.R.; De Leo, F.C. Hawaiian hotspots: Enhanced megafaunal abundance and diversity in submarine canyons on the oceanic islands of Hawaii. *Mar. Ecol.* **2010**, *31*, 183–199. [CrossRef]
10. Fernandez-Arcaya, U.; Ramirez-Llodra, E.; Aguzzi, J.; Allcock, A.L.; Davies, J.S.; Dissanayake, A.; Harris, P.; Howell, K.; Huvenne, V.A.I.; Macmillan-Lawler, M.; et al. Ecological Role of Submarine Canyons and Need for Canyon Conservation: A Review. *Front. Mar. Sci.* **2017**, *4*, 5. [CrossRef]
11. Farrugio, H. A refugium for the spawners of exploited Mediterranean marine species: The canyons of the continental slope of the Gulf of Lion. In *Mediterranean Submarine Canyons: Ecology and Governance*; Würtz, M., Ed.; International Union for Conservation of Nature: Gland, Switzerland, 2012; pp. 45–50.
12. O'Neill, F.G.; Summerbell, K. The mobilization of sediment by demersal otter trawls. *Mar. Pollut. Mar.* **2011**, *62*, 1088–1097. [CrossRef] [PubMed]
13. Martín, J.; Puig, P.; Palanques, A.; Ribó, M. Trawling-induced daily sediment resuspension in the flank of a Mediterranean submarine canyon. *Deep Sea Res. Part II Top. Stud. Oceanogr.* **2014**, *104*, 174–183. [CrossRef]

14. Martín, J.; Puig, P.; Masqué, P.; Palanques, A.; Sánchez-Gómez, A. Impact of bottom trawling on deep-sea sediment properties along the flanks of a submarine canyon. *PLoS ONE* **2014**, *9*, e104536. [CrossRef] [PubMed]
15. O'Neill, F.G.; Ivanovic, A. The physical impact of towed demersal fishing gears on soft sediments. *ICES J. Mar. Sci.* **2016**, *73*, i5–i14. [CrossRef]
16. Depestele, J.; Ivanovic, A.; Degrendele, K.; Esmaeili, M.; Polet, H.; Roche, M.; Summerbell, K.; Teal, L.R.; Vanelslander, B.; O'Neill, F.G. Measuring and assessing the physical impact of beam trawling. *ICES J. Mar. Sci.* **2016**, *73*, i15–i26. [CrossRef]
17. Daly, E.; Johnson, M.P.; Wilson, A.M.; Gerritsen, H.D.; Kiriakoulakis, K.; Allcock, A.L.; White, M. Bottom trawling at Whittard Canyon: Evidence for seabed modification, trawl plumes and food source heterogeneity. *Prog. Oceanogr.* **2018**, *169*, 227–240. [CrossRef]
18. Palanques, A.; Martín, J.; Puig, P.; Guillén, J.; Company, J.B.; Sardà, F. Evidence of sediment gravity flows induced by trawling in the Palamós (Fonera) submarine canyon (northwestern Mediterranean). *Deep Sea Res. I Oceanogr. Res. Pap.* **2006**, *53*, 201–214. [CrossRef]
19. Martín, J.; Palanques, A.; Puig, P. Near-bottom horizontal transfer of particulate matter in the Palamós Submarine Canyon (NW Mediterranean). *J. Mar. Res.* **2007**, *65*, 193–218. [CrossRef]
20. Puig, P.; Canals, M.; Company, J.B.; Martín, J.; Amblas, D.; Lastras, G.; Palanques, A. Ploughing the deep sea floor. *Nature* **2012**, *489*, 286–289. [CrossRef]
21. Chronis, G.; Lykousis, V.; Georgopoulos, D.; Zervakis, V.; Stavrakakis, S.; Poulos, S. Suspended particulate matter and nepheloid layers over the southern margin of the Cretan Sea (NE Mediterranean): Seasonal distribution and dynamics. *Prog. Oceanogr.* **2000**, *46*, 163–185. [CrossRef]
22. Wilson, A.M.; Kiriakoulakis, K.; Raine, R.; Gerritsen, H.D.; Blackbird, S.; Allcock, A.L.; White, M. Anthropogenic influence on sediment transport in the Whittard Canyon, NE Atlantic. *Mar. Pollut. Bull.* **2015**, *101*, 320–329. [CrossRef] [PubMed]
23. Arjona-Camas, M.; Puig, P.; Palanques, A.; Emelianov, M.; Durán, R. Evidence of trawling-induced resuspension events in the generation of nepheloid layers in the Foix submarine canyon (NW Mediterranean). *J. Mar. Syst.* **2019**, *196*, 86–96. [CrossRef]
24. Arjona-Camas, M.; Puig, P.; Palanques, A.; Durán, R.; White, M.; Paradis, S.; Emelianov, M. Natural vs. trawling-induced water turbidity and suspended sediment transport variability within the Palamós Canyon (NW Mediterranean). *Mar. Geophys. Res.* **2021**, *42*, 38. [CrossRef]
25. Martín, J.; Puig, P.; Palanques, A.; Masqué, P.; García-Orellana, J. Effect of commercial trawling on the deep sedimentation in a Mediterranean submarine canyon. *Mar. Geol.* **2008**, *252*, 150–155. [CrossRef]
26. Puig, P.; Martín, J.; Masqué, P.; Palanques, A. Increasing sediment accumulation rates in La Fonera (Palamós) submarine canyon axis and their relationship with bottom trawling activities. *Geophys. Res. Lett.* **2015**, *42*, 8106–8113. [CrossRef]
27. Paradis, S.; Puig, P.; Masqué, P.; Juan-Díaz, X.; Martín, J.; Palanques, A. Bottom trawling along submarine canyons impacts deep sedimentary regimes. *Sci. Rep.* **2017**, *7*, 43332. [CrossRef] [PubMed]
28. Paradis, S.; Puig, P.; Sánchez-Vidal, A.; Masqué, P.; García-Orellana, J.; Calafat, A.; Canals, M. Spatial distribution of sedimentation-rate increases in Blanes Canyon caused by technification of bottom trawling fleet. *Prog. Oceanogr.* **2018**, *169*, 241–252. [CrossRef]
29. Paradis, S.; Masqué, P.; Puig, P.; Juan-Diaz, X.; Gorelli, G.; Company, J.B.; Palanques, A. Enhancement of sedimentation rates in the Foix Canyon after the renewal of trawling fleets in the early XXIst century. *Deep Sea Res. Part I Oceanogr. Res. Pap.* **2018**, *132*, 51–59. [CrossRef]
30. Lo Iacono, C.; Sulli, A.; Agate, M.; Lo Presti, V.; Pepe, F.; Catalano, R. Submarine canyon morphologies in the Gulf of Palermo (Southern Tyrrhenian Sea) and possible implications for geo-hazard. *Mar. Geophys. Res.* **2011**, *32*, 127–138. [CrossRef]
31. Lo Iacono, C.; Sulli, A.; Agate, M. Submarine canyons of north-western Sicily (Southern Tyrrhenian Sea): Variability in morphology, sedimentary processes, and evolution on a tectonically active margin. *Deep-Sea Res. Part II Top. Stud. Oceanogr.* **2014**, *104*, 93–105. [CrossRef]
32. Paradis, S.; Lo Iacono, C.; Masqué, P.; Puig, P.; Palanques, A.; Russo, T. Evidence of large increases in sedimentation rates due to fish trawling in submarine canyons of the Gulf of Palermo (SW Mediterranean). *Mar. Pollut. Bull.* **2021**, *172*, 112861. [CrossRef] [PubMed]
33. Palanques, A.; Paradis, S.; Puig, P.; Masqué, P.; Lo Iacono, C. Effects of bottom trawling on trace metal contamination of sediments along the submarine canyons of the Gulf of Palermo (southwestern Mediterranean). *Sci. Total Environ.* **2022**, *814*, 152658. [CrossRef]
34. Di Leonardo, R.; Bellanca, A.; Capotondi, L.; Cundy, A.; Neri, R. Possible impacts of Hg and PAH contamination on benthic foraminiferal assemblages: An example from the Sicilian coast, Central Mediterranean. *Sci. Total Environ.* **2007**, *388*, 168–183. [CrossRef] [PubMed]
35. Rizzo, S.; Basile, S.; Caruso, A.; Cosentino, C.; Tranchina, L.; Brai, M. Dating of a sediment Core by 210Pbex method and pb pollution chronology in the Palermo gulf (Italy). *Water Air Soil Pollut.* **2009**, *202*, 109–120. [CrossRef]
36. Mannina, G.; Viviani, G. Water quality modelling for ephemeral rivers: Model development and parameter assessment. *J. Hydrol.* **2010**, *393*, 186–196. [CrossRef]
37. Tranchina, L.; Basile, S.; Brai, M.; Caruso, A.; Cosentino, C.; Miccichè, S. Distribution of heavy metals in marine sediments of Palermo Gulf (Sicily, Italy). *Water Air Soil Pollut.* **2008**, *191*, 245–256. [CrossRef]
38. Chiocci, F.L.; Ridente, D. Regional-scale seafloor mapping and geohazard assessment. The experience from the Italian project MaGIC (Marine Geohazards along the Italian Coasts). *Mar. Geophys. Res.* **2011**, *32*, 13–23. [CrossRef]
39. De la Vara, A.; Parras-Berrocal, I.M.; Izquierdo, A.; Sein, D.V.; Cabos, W. Climate change signal in the ocean circulation of the Tyrrhenian Sea. *Earth Syst. Dynam.* **2002**, *13*, 303–319. [CrossRef]

40. Pinardi, N.; Masetti, E. Variability of the large scale general circulation of the Mediterranean Sea from observations and modelling: A review. *Palaeogeogr. Palaeoclimatol. Palaeoecol.* **2000**, *158*, 153–173. [CrossRef]
41. Astraldi, M.; Gasparini, G.P.; Vetrano, A.; Vignudelli, S. Hydrographic characteristics and interannual variability of water masses in the central Mediterranean: A sensitivity test for long-term changes in the Mediterranean Sea. *Deep Sea Res. Part I Oceanogr. Res. Pap.* **2002**, *49*, 661–680. [CrossRef]
42. Millot, C. Circulation in the western Mediterranean Sea. *J. Mar. Syst.* **1999**, *20*, 423–442. [CrossRef]
43. Sparnocchia, S.; Gasparini, G.P.; Astraldi, M.; Borghini, M.; Pistek, P. Dynamics and mixing of the Eastern Mediterranean outflow in the Tyrrhenian basin. *J. Mar. Syst.* **1999**, *20*, 301–317. [CrossRef]
44. Robinson, A.R.; Leslie, W.G.; Thecharis, A.; Lascaratos, A. Mediterranean Sea circulation. *Encycl. Ocean Sci.* **2001**, *1*, 19. [CrossRef]
45. Budillon, G.; Gasparini, G.P.; Schroeder, K. Persistence of an eddy signature in the central Tyrrhenian basin. *Deep Sea Res. Part II Top. Stud. Oceanogr.* **2009**, *56*, 713–724. [CrossRef]
46. Astraldi, M.; Gasparini, G.P. The seasonal characteristics of the circulation in the Tyrrhenian Sea. *Seas. Interannual Var. West. Mediterr. Sea* **1994**, *46*, 661–680. [CrossRef]
47. Vetrano, A.; Napolitano, E.; Iacono, R.; Schroeder, K.; Gasparini, G.P. Tyrrhenian Sea circulation and water mass fluxes in spring 2004: Observations and model results. *J. Geophys. Res. Ocean.* **2010**, *115*, C06023. [CrossRef]
48. Iacono, R.; Napolitano, E.; Marullo, S.; Artale, V.; Vetrano, A. Seasonal variability of the Tyrrhenian Sea surface geostrophic circulation as assessed by altimeter data. *J. Phys. Oceanogr.* **2013**, *43*, 1710–1732. [CrossRef]
49. Rhein, M.; Send, U.; Klein, B.; Krahmann, G. Interbasin deep water exchange in the western Mediterranean. *J. Geophys. Res. Ocean.* **1999**, *104*, 23495–23508. [CrossRef]
50. Fuda, J.L.; Etope, G.; Millot, C.; Favali, P.; Calcara, M.; Smriglio, G.; Boschi, E. Warming, salting and origin of the Tyrrhenian Deep Water. *Geophys. Res. Lett.* **2002**, *29*, 4-1–4-4. [CrossRef]
51. Millot, C. Another description of the Mediterranean Sea outflow. *Prog. Oceanogr.* **2009**, *66*, 231–250. [CrossRef]
52. Falco, P.; Trani, M.; Zambianchi, E. Water mass structure and deep mixing processes in the Tyrrhenian Sea: Results from the VECTOR project. *Deep Sea Res. Part I Oceanogr. Res. Pap.* **2016**, *113*, 7–21. [CrossRef]
53. Menna, M.; Poulain, P.M.; Ciani, D.; Doglioli, A.; Notarstefano, G.; Gerin, R.; Rio, M.H.; Santoleri, R.; Gauci, A.; Drago, A. New insights of the Sicily Channel and southern Tyrrhenian Sea variability. *Water* **2019**, *11*, 1355. [CrossRef]
54. Istituto Idrografico della Marina. *Atlante della Correnti Superficiali dei Mari Italiani*; Istituto Idrografico della Marina: Genoa, Italy, 1982.
55. Solomon, O.M.; Larson, D.R.; Paulter, N.G. Comparison of some algorithms to estimate the low and high state level of pulses. In *Proceedings of the IMTC 2001, Proceedings of the 18th IEEE Instrumentation and Measurement Technology Conference. Rediscovering Measurement in the Age of Informatics (Cat. No.01CH 37188), Budapest, Hungary, 21–23 May 2001*; IEEE: Piscataway, NJ, USA, 2001; Volume 1, pp. 96–101. [CrossRef]
56. Kalkan, E. spikeRemoval. MATLAB Central File Exchange. 2024. Available online: https://www.mathworks.com/matlabcentral/fileexchange/69614-spikeremoval (accessed on 1 May 2024).
57. Carlson, D.F.; Muscarella, P.A.; Gildor, H.; Lipphardt, B.L.; Fredj, E. How useful are progressive vector diagrams for studying coastal ocean transport? *Limnol. Oceanogr. Methods* **2010**, *8*, 98–106. [CrossRef]
58. Schlitzer, R. Ocean Data View. 2010. Available online: https://odv.awi.de (accessed on 19 October 2022).
59. Troupin, C.; Barth, A.; Sirjacobs, D.; Ouberdous, M.; Brankart, J.M.; Brasseur, P.; Rixen, M.; Alvera-Azcárate, A.; Belounis, M.; Capet, A.; et al. Generation of analysis and consistent error fields using the Data Interpolating Variational Analysis (DIVA). *Ocean Model.* **2012**, *52*, 90–101. [CrossRef]
60. Korres, G.; Ravdas, M.; Zacharioudaki, A.; Denaxa, D.; Sotiropoulou, M. *Mediterranean Sea Waves Reanalysis (CMEMS Med-Waves, MedWAM3 System)*, version 1; [Data Set]; Copernicus Monitoring Environment Marine Service (CMEMS): Ramonville-Saint-Agne, France, 2021. [CrossRef]
61. Korres, G.; Ravdas, M.; Zacharioudaki, A. *Mediterranean Sea Waves Hindcast (CMEMS MED-Waves)*; [Data Set]; Copernicus Monitoring Environment Marine Service (CMEMS): Ramonville-Saint-Agne, France, 2019. [CrossRef]
62. European Commission. Commission regulation (EC) No. 2244/2003 of 18 December 2003 laying down detailed provisions regarding satellite-based Vessel Monitoring Systems. *Off. J. Eur. Union* **2003**, *L333*, 17–27. Available online: http://data.europa.eu/eli/reg/2003/2244/oj (accessed on 19 October 2022).
63. Lambert, G.I.; Jennings, S.; Hiddink, J.G.; Hintzen, N.T.; Hinz, H.; Kaiser, M.J.; Murray, L.G. Implications of using alternative methods of vessel monitoring system (VMS) data analysis to describe fishing activities and impacts. *ICES J. Mar. Sci.* **2012**, *69*, 682–693. [CrossRef]
64. Russo, T.; D'Andrea, L.; Parisi, A.; Cataudella, S. VMSbase: An R-package for VMS and logbook data management and analysis in fisheries ecology. *PLoS ONE* **2014**, *9*, e100195. [CrossRef]
65. Mendoza, E.T.; Jiménez, A.A. Vulnerability assessment to coastal storms at a regional scale. *Coast. Eng.* **2008**, *5*, 4154–4166. [CrossRef]
66. Paradis, S.; Pusceddu, A.; Masqué, P.; Puig, P.; Moccia, D.; Russo, T.; Lo Iacono, C. Organic matter contents and degradation in a highly trawled area during fresh particle inputs (Gulf of Castellammare, southwestern Mediterranean). *Biogeosciences* **2019**, *16*, 4307–4320. [CrossRef]
67. Linders, T.; Nilsson, P.; Wikström, A.; Sköld, M. Distribution and fate of trawling-induced resuspension sediments in a marine protected area. *ICES J. Mar. Sci.* **2018**, *75*, 785–795. [CrossRef]
68. Pierini, S. Topographic Rossby modes in the Strait of Sicily. *J. Geophys. Res. Ocean.* **1996**, *101*, 6429–6440. [CrossRef]

69. Flexas, M.M.; Durrieu de Madron, X.; Garcia, M.A.; Canals, M.; Arnau, P. Flow variability in the Gulf of Lions during the MATER HFF experiment (March–May 1997). *J. Mar. Syst.* **2002**, *33*, 197–214. [CrossRef]
70. Palanques, A.; García-Ladona, E.; Gomis, D.; Martín, J.; Macros, M.; Pascual, A.; Puig, P.; Gili, J.M.; Emelianov, M.; Montserrat, S.; et al. General patterns of circulation, sediment fluxes and ecology of the Palamós (La Fonera) submarine canyon, northwestern Mediterranean. *Prog. Oceanogr.* **2005**, *66*, 89–119. [CrossRef]
71. Puig, P.; Palanques, A.; Orange, D.L.; Lastras, G.; Canals, M. Dense shelf water cascades and sedimentary furrow formation in the Cap de Creus Canyon, northwestern Mediterranean Sea. *Cont. Shelf Res.* **2008**, *28*, 2017–2030. [CrossRef]
72. Van Haren, G.; Gostiaux, L. Large internal waves advection in very weakly stratified deep Mediterranean waters. *Geophys. Res. Lett.* **2011**, *38*, 22. [CrossRef]
73. Bonaldo, D.; Orlic, M.; Carniel, S. Framing Continental Shelf Waves in the southern Adriatic Sea, a further flushing factor beyond dense water cascading. *Sci. Rep.* **2018**, *8*, 660. [CrossRef] [PubMed]
74. Sammari, C.; Millot, C.; Prieur, L. Aspects of the seasonal and mesoscale variabilities of the Northern Current in the western Mediterranean Sea inferred from the PROLIG-2 and PROS-6 experiments. *Deep Sea Res. Part I Oceanogr. Res. Pap.* **1995**, *42*, 893–917. [CrossRef]
75. Ribó, M.; Puig, P.; van Haren, H. Hydrodynamics over the Gulf of Valencia continental slope and their role in sediment transport. *Deep Sea Res. Part I Res. Oceanogr. Pap.* **2015**, *95*, 54–66. [CrossRef]
76. McPhee-Shaw, E.E.; Kunze, E. Boundary layer intrusions from a sloping bottom: A mechanism for generating intermediate nepheloid layers. *J. Geophys. Res. Ocean.* **2002**, *107*, 3-1–3-16. [CrossRef]
77. McPhee-Shaw, E.E. Boundary-interior exchange: Reviewing the idea that internal-wave mixing enhances lateral dispersal near continental margins. *Deep Sea Res. Part II Top. Stud. Oceanogr.* **2006**, *53*, 42–59. [CrossRef]
78. Richardson, K.; Gunn, R.; Wilcox, C.; Hardesty, B.D. Understanding causes of gear loss provides a sound basis for fisheries management. *Mar. Policy.* **2018**, *96*, 278–284. [CrossRef]
79. van Haren, H.; Millot, C. Rectiliniar and circular inertial motions in the Western Mediterranean Sea. *Deep Sea Res. Part I Oceanogr. Res. Pap.* **2004**, *51*, 1441–1455. [CrossRef]
80. Hosegood, P.; van Haren, H. Near-bed solibores over the continental slope in the Faroe-Shetland Channel. *Deep Sea Res. Part II Top. Stud. Oceanogr.* **2004**, *51*, 2943–2971. [CrossRef]
81. Liu, J.T.; Wang, Y.H.; Lee, I.H.; Hsu, R.T. Quantifying tidal signatures of the benthic nepheloid layer in Gaoping Submarine Canyon in Southern Taiwan. *Mar. Geol.* **2010**, *27*, 119–130. [CrossRef]